



WPI

High Energy Passive Solar System Design in Santa Fe, New Mexico

A Major Qualifying Project

Submitted to the faculty of Worcester Polytechnic Institute

In partial fulfillment of the requirements for the degree of Bachelor of Science

Submitted by:

Sarah Abatiello, Maren Cork, Emma Driscoll, Sydney Smith, Jade Veth, and Effelia Dawn Warden

April 27, 2023

Project Advisors:

Selcuk Guceri, Stephen Kmiotek, and Elisabeth Stoddard

This report represents the work of one or more WPI undergraduate students submitted to the faculty as evidence of completion of a degree requirement. WPI routinely publishes these reports on the web without editorial or peer review. For more information about the projects program at WPI, please see <http://www.wpi.edu/academics/ugradstudies/project-learning.html>.

ABSTRACT

This project explored integrating phase change material (PCM) to increase energy storage capacity of building materials in Trombe walls, a passive solar system. PCMs absorb and release thermal energy during the changing of phases. For this project, a water-based gel was explored, contained in PVC tubing within a standard modular concrete brick. A brick configuration with an 8.5% increase in heat capacity was found through thermal tests. These results combined with solar modeling to create a thermal simulation yielded a 9.6% increase in useful passive energy release compared to standard Trombe walls, and a cost analysis predicted 22% savings in heating costs. Finally, policy incentives and funding mechanisms were discussed to aid the implementation of PCM-containing passive solar systems.

TABLE OF CONTENTS

ABSTRACT	1
TABLE OF CONTENTS	2
TABLE OF FIGURES	3
TABLE OF TABLES	3
AUTHORSHIP	4
ACKNOWLEDGEMENTS	4
1. INTRODUCTION	5
2. BACKGROUND	6
2.1 Modeling Solar Position	7
2.2 Modeling the Angle of Incidence	9
2.3 Modeling Solar Intensity	9
2.4 Solar Transmissivity	10
2.5 Thermal Properties of Phase Change Materials	11
3. METHODOLOGY	13
3.1 Understanding Solar Intensity	13
3.2 Development of Kinetics of Solar Radiation	14
3.3 Exploration of Materials and Containment	15
3.4 Determining Heat Capacity of the Bricks	16
3.5 Development of Thermal Simulation using SolidWorks	20
4. RESULTS and DISCUSSION	21
4.1 Heat Capacity of Bricks	21
4.2 Solar Intensity Modeling	23
4.3 Thermal Simulation/Cycle	24
4.4 Cost Analysis	25
4.5 Limitations	26
4.6 Passive Solar Retention and Release	27
4.6.1 New Builds	28
4.6.2 Retrofits	30
5. CONCLUSIONS and RECOMMENDATIONS	33
5.1 Future Work and Applications	33
5.2 Recommendations for Policy Incentives and Funding Mechanisms	34
REFERENCES	35
APPENDICES	41
Appendix A. Solar Intensity Data	41
Appendix B. Solar Intensity Graphs and Equations	42
Appendix C. Composite Mold Details	45
Appendix D. Testing Apparatus Details	46

Appendix E. Sample Calculations for Heat Capacity	50
Appendix F. MATLAB Flux Time Curve Generation Code	51
Appendix G. Simulation Results Data	61

TABLE OF FIGURES

<i>Figure 1.</i> Schematic of the Trombe Wall, a passive solar system (Quesada et al., 2012).	6
<i>Figure 2.</i> A diagram displaying the Zenith and Azimuth angles used to denote the Sun's position.	7
<i>Figure 3.</i> Sunray intensity based on Earth's location (Harris, 2018).	10
<i>Figure 4.</i> Solar rays with respect to DNI, GHI and DHI (Singh, 2020).	14
<i>Figure 5.</i> Schematic of brick dimensions.	17
<i>Figure 6.</i> Tubing configurations for brick casting.	18
<i>Figure 7.</i> Brick testing apparatus.	19
<i>Figure 8.</i> An example time curve of inbound heat flux for January, showing the inflection point used to determine the start of the time range energy released was compared over.	21
<i>Figure 9.</i> Calculated heat capacity of composite brick based on containment diameter.	23
<i>Figure 10.</i> Chart showing energy in and out of the brick for a standard Trombe wall brick simulated in January.	25

TABLE OF TABLES

<i>Table 1.</i> Rigid PVC Tubing Specifications.	16
<i>Table 2.</i> Heat Capacity for Bricks with Different Materials.	22
<i>Table 3.</i> Average heat capacity of composite bricks, depending on tubing containment diameter.	23
<i>Table 4.</i> The table displaying the relative increase of energy released for PCM bricks compared to a standard Trombe wall brick	25

AUTHORSHIP

Our project team was divided into two main subsections, one focused on solar modeling and the other on the design and testing of brick material. The solar modeling group included Effelia Warden, Sarah Abatiello, and Sydney Smith who were responsible for all solar position, intensity, and transmissivity calculations which resulted in a comprehensive solar model for Santa Fe, New Mexico. The material group included Emma Driscoll, Jade Veth, and Maren Cork who were responsible for the exploration of PCM, containment, and the testing of the thermal properties of the composite material. One of our team members, Sydney Smith, has a second major, Environmental & Sustainability Studies. As part of her MQP for the second major, she wrote section 4.6 and 5.2 about policy incentives, funding mechanisms, and recommendations.

Due to the collaborative nature of the project, the entire group collaborated to bring together the two sections into a comprehensive report. This report can be seen as a joint effort from all team members, with each section written and edited by multiple members.

ACKNOWLEDGEMENTS

We would like to extend our gratitude to the members of the WPI community who aided us in the completion of our Major Qualifying Project. The support and guidance of our advisors, Selcuk Guceri, Stephen Kmiotek, and Elisabeth Stoddard were especially appreciated.

Additionally, assistance from Ian Anderson and Doug White of the chemical engineering department was instrumental in the successful testing of our product. Finally, we would like to thank Ahmet Sabuncu for his support with our Arduino data logging setup.

1. INTRODUCTION

As individuals look for more ways to save money from increasing heating and cooling costs, a solution can be found in passive solar systems. These systems convert sunlight into heat and allow for air movement to heat and cool homes or businesses without the use of additional mechanical or electrical devices. With its obvious abundance, ways to actively harness the sun's light to produce energy have been explored, but they could be improved. A well-known passive solar system is the Trombe wall which "is made of dark-colored building materials and covered with vertical glass, whereby ventilated air can circulate between the wall and the glazing" (Xiong et al., 2022). By experimenting with the different components of a Trombe wall, a more efficient system can be produced. Specifically, our goal was to explore the practicality of integrating phase change material (PCM) to increase energy storage capacity for building materials in passive solar systems.

We concentrated our solar modeling research on a specific location, Santa Fe, New Mexico. Using regional solar intensity data and principles of solar position tracking and heat transmission through glazing, we generated time curves of heat flux into the Trombe wall. We also investigated the performance of different PCMs for heat storage and containment strategies in concrete.

In this report, we detail our approach to designing and developing a proof of concept modular brick that incorporates PCM to yield a higher energy storage capacity than one without. We explored two main materials and three different containment options in this report. The two materials were clay and gel in hot/cold packs typically used for pain relief. These materials are cheap, readily available, and have a high heat capacity, making them viable options for our project. After casting bricks, we tested them in a calorimeter-like apparatus designed to calculate the heat capacity of the composite bricks. Our first set of trials aimed to determine the material that led to a higher heat capacity and our second set aimed to determine an optimal diameter for the containment of the material. With this energy storage capacity, a simulation was run with solar time curve data to evaluate the thermal responses of different brick configurations. Results were used to estimate the energy and cost savings of the optimal brick configuration.

Finally, research and analysis were done to determine policy incentives and funding mechanisms that exist for Trombe walls. We looked into differing policies and funding for both new builds and retrofits. We investigated the implementation of regular Trombe walls, modified Trombe walls, and PCM retrofit panels. Based on the results, conclusions, and findings from this section of the report, we made recommendations to incorporate passive solar and Trombe wall language explicitly into tax incentives and education programs currently available in the state of New Mexico.

The main goals of our project were to develop a tool to model solar behavior in Santa Fe, to select a material to increase passive solar capture, and to combine these aspects to create a thermal simulation of our wall in New Mexico. Finally, we aimed to suggest policies to increase the implementation of passive solar systems containing PCM.

2. BACKGROUND

Passive solar systems harness the sun's energy to heat a space without any mechanical or electrical work. Passive solar requires an integrative design with the environment and solar position to optimize efficiency and supplement the main heating and cooling systems in a building. The fundamental considerations for these systems are window position, thermal mass, distribution, and control (*Passive Solar Homes*, n.d.). Solar energy or heat is transmitted through unobstructed windows facing the south in the northern hemisphere and facing north in the southern hemisphere. Heat is stored in a thermal mass, usually, a concrete or stone wall that doubles as a structural element, which stores heat during the day when solar insolation is high and releases heat at night when the temperature is cooler. Thermal mass in a building reduces temperature fluctuations and heating and cooling loads (Donev, n.d.). Convection, whether passive or forced, is often used to distribute the heat collected and stored in the thermal mass to the entire space. Shading strategies are useful to control mechanisms for solar energy collection. An example of a passive solar system is the Trombe wall shown below.

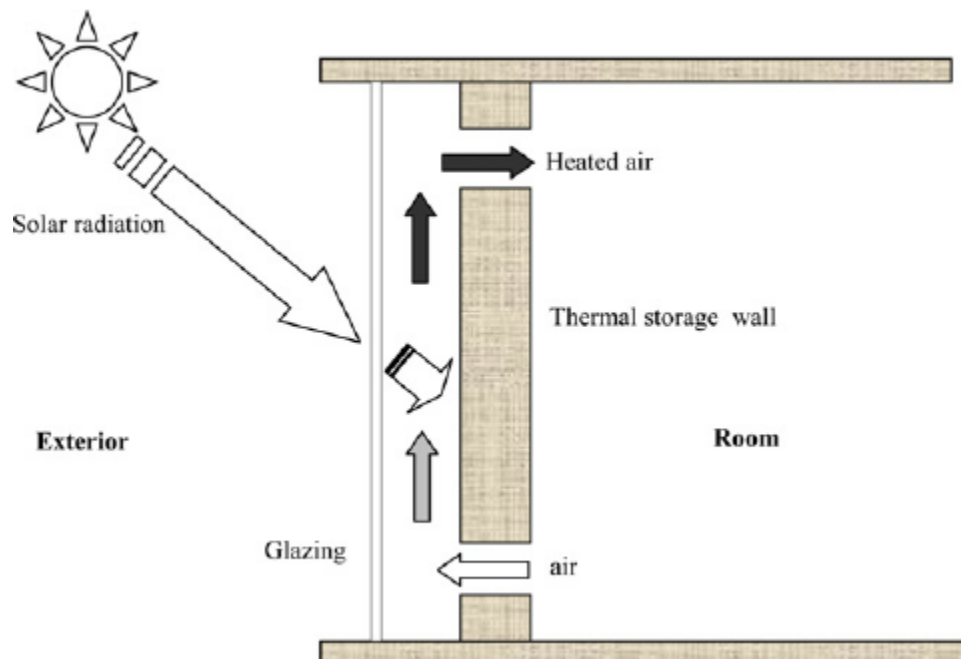


Figure 1. Schematic of the Trombe Wall, a passive solar system (Quesada et al., 2012).

Figure 1 shows a schematic of a Trombe wall facing the sun. Solar radiation transmits through the glazing and is absorbed by the thermal mass. The glazing traps the heat in an air gap that is between 0.75 to 6.0 inches from the thermal mass. As solar energy waves pass through the glass, they are reflected from the thermal mass with longer wavelengths that do not pass through the glass again. (*How Does a Trombe Wall Work?* | *ArchDaily*, n.d.). A selective absorber material such as a metal foil secured to the outside surface of the thermal storage wall will also increase absorption and decrease light emittance off the wall. The thick thermal mass, between 8 to 16 inches thick, will store heat for the day and release heat at night. A thicker wall will delay heat

from entering the interior rooms by eight to ten hours, so the inside is cool during the hot day and warmer during the cool night (“Building a Better Trombe Wall,” n.d.). Figure 1 also shows a passive convection element where vents at the bottom and top of the thermal mass allow cool air from the room to pass through the air gap and be heated by solar radiation.

Based on how Trombe walls function, they are a useful element to incorporate into buildings to help with heating, cooling, and ventilation. A major benefit is their ability to reduce the heating and cooling loads on the main mechanical systems. At the Zion National Park visitor center, a study by the National Renewable Energy Laboratory (NREL) found that the Trombe wall integrated into its building supplied 20% of annual heating (Pless & Torcellini, 2004). Further design choices regarding the color and material of the glazing and thermal mass could increase efficiency; however, Trombe walls are most effective in year-round sunny environments. They are most applicable in locations that boast high solar gains in the day and low temperatures at night, but there are various Trombe wall designs adapted to suit different climatic needs (Bhamare et al., 2019). Santa Fe, New Mexico was selected as the experimental location for this project due to its semi-arid climate with four distinct seasons. It experiences sunshine throughout the year, on average 325 days per year, and has mild winters and low annual rainfall (*Climate | Santa Fe Chamber of Commerce | Santa Fe, NM*, n.d.). Over the year, Santa Fe temperatures typically vary from -8°C to 30°C (Aladin, n.d.).

2.1 Modeling Solar Position

In order to evaluate the effectiveness of a Trombe wall design, the angle and intensity of solar rays must be taken into account. The position of the sun in the sky is typically modeled by considering a hemispherical dome around the horizontal flat plane of the ground. Within this dome, the position of the sun is indicated by two angles, the azimuth angle, and either the elevation or zenith angle (Brownson, n.d.; Honsberg & Bowden, n.d.; Sena, 2021a). The zenith and elevation are complementary angles — the zenith angle is measured vertically, and the elevation angle is measured from the ground. These angles range from 0 to 180 and -90 to 90 degrees respectively. The azimuth angle is typically measured eastward from North and ranges from 0 to 360 degrees. These angles are shown in Figure 2.

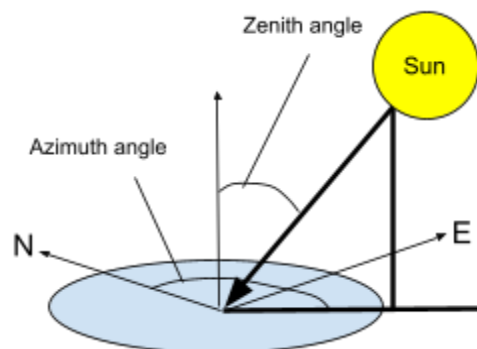


Figure 2. A diagram displaying the Zenith and Azimuth angles used to denote the Sun's position.

The variation of the azimuth and zenith angles have been thoroughly modeled and can be calculated with information about the position on the Earth of interest, as well as the date and time. The effect of date and time is modeled by the inclusion of two factors in the equations for azimuth and zenith angles: the declination angle and the hour angle (Sena, 2021b).

The declination angle (δ) is the angle between inbound solar radiation and the Earth's equator, factoring variance throughout each year caused by the Earth's axis of rotation being offset by 23.4 degrees (the maximum declination). Formulas to calculate declination use the decimal amount of days (d) since January 1st at 0:00 Coordinated Universal Time (UTC), the time zone of Earth's prime meridian. It is calculated using the following formulas, where the declination angle will be output in degrees (R. Milne, 1921; Zerubavel, 1982).

$$\delta = -23.44^\circ * \cos\left(\frac{360}{365}(d + 10)\right) \text{ [degrees]} \quad (1)$$

Where d is expressed as:

$$d = \text{days since Jan 1st (Local time)} + (LT - \Delta T_{UTC}) / (24\text{hr}) \text{ [days]}$$

Where LT is the local time, and ΔT_{UTC} is the difference between local time and UTC.

The hour angle is a more complicated formulation, which takes into account several correction factors to express local time (LT) as local solar time (LST), which is a time scale where the sun is overhead at noon and is used to calculate the hour angle (Sena, 2021b).

The first of these corrections is the Equation of Time, which corrects for the Earth's axial tilt and orbital eccentricities. The equation for the Equation of time is expressed below.

$$EoT = 9.87\sin(2B) - 7.53\cos(B) - 1.5\sin(B) \text{ [minutes]} \quad (2)$$

Where B is expressed as:

$$B = \frac{360}{365}(d - 81) \text{ [degrees]} \quad (3)$$

To account for the difference in time zone from UTC, the local standard time meridian ($LSTM$) is used as a reference and is calculated as follows:

$$LSTM = 15^\circ \Delta T_{UTC} \text{ [degrees]} \quad (4)$$

The $LSTM$, EoT , and longitude ($Long$) are used to calculate the Time Correction Factor (TC). The time correction factor uses the knowledge that the Earth rotates one degree in four minutes to express how the local solar time will vary due to the longitudinal position within the local time zone, as well as including the effect of the EoT (Sena, 2021b).

$$TC = 4(Long - LSTM) + EoT \text{ [minutes]} \quad (5)$$

The time correction factor and local time can then be used to calculate the local solar time as follows (Quesada et al., 2012; Sena, 2021a):

$$LST = LT + TC/60 \quad (6)$$

Which is used to find the hour angle in the formula:

$$h = 15^{\circ} * (LST - 12) [degrees] \quad (7)$$

With these correction factors and the local latitude (Φ) the solar zenith angle (θ_s) and the solar azimuth angle (ϕ_s)- both in degrees- are calculated with the following equations (Honsberg & Bowden, n.d.):

$$\cos\theta_s = \sin\Phi\sin\delta + \cos\Phi\cos\delta\cos(h) \quad (8)$$

$$\cos\phi_s = \frac{\sin\delta\cos\Phi - \cos\delta\sin\Phi\cos(h)}{\sin\theta_s} \quad (9)$$

2.2 Modeling the Angle of Incidence

While the zenith and azimuth angles are helpful to display the position of the sun at a given location, they are not as helpful when working with irradiation inbound to an oriented surface at that location. For a flat surface, the angle of incidence (θ_c) between the incoming solar irradiation and the normal vector of a flat surface can be calculated using the same factors used for the zenith and azimuth angle. To include the effects of the orientation of the surface, there are two more factors used: the surface tilt (β) and the surface azimuth (γ). The surface tilt measures the angle between the surface and the ground, ranging from 0° for a horizontal surface to 90° for a vertical surface such as a typical house wall. The surface azimuth measures the angle of the projected normal vector in the ground plane, much like the solar azimuth angle. However, in the following equation for the angle of incidence, unlike solar azimuth, collector azimuth is measured from the South, where the West is positive (Brownson, n.d.):

$$\begin{aligned} \cos\theta_c = & \sin(\Phi)\sin(\delta)\cos(\beta) - \cos(\Phi)\sin(\delta)\sin(\beta)\cos(\gamma) + \cos(\Phi)\cos(\delta)\cos(\beta)\cos(h) + \\ & \dots + \sin(\Phi)\cos(\delta)\sin(\beta)\cos(\gamma)\cos(h) + \cos(\delta)\sin(\beta)\sin(\gamma)\sin(h) \end{aligned} \quad (10)$$

2.3 Modeling Solar Intensity

In addition to solar position and angle of incidence, solar intensity plays a large role in passive solar systems. Throughout the year, the sun can reach every part of the earth. The amount of radiation from sun rays depends on the location, time of day, the season, the landscape, and the weather (*Solar Radiation Basics*, n.d.). The sun is at its highest strength when its rays are vertical or directly overhead to the area of interest. For this reason, the location is important. The sun's location in relation to the area of interest is the zenith angle. Thus, a larger zenith angle corresponds to a higher solar intensity (Tycorun, 2022).

Similar to the zenith angle, the latitudes of locations are important to sun radiation reaching the earth. Earth is divided into 3 major weather zones: polar, temperate, and tropical, pictured below in Figure 3. The polar zones refer to the Arctic and Antarctic Circles where temperatures are severely cold. The temperate zone falls below the arctic circle to the Tropic of Cancer along with falling above the antarctic circle and stopping at the Tropic of Capricorn. Temperatures in these

areas range between 23.5 degrees Celsius to 66.5 degrees Celsius which is considerably warmer than the polar zone. Lastly is the tropical zone consisting of the area between the Tropic of Capricorn and the Tropic of Cancer. This area is considerably warmer and varies from wet regions to drier climates. Distance from the equator will impact how the sun's rays hit Earth. Due to the earth's tilt on its axis, the sun's rays will hit at a near-vertical angle on the equator, which becomes more shallow as the distance from the equator increases. The shallower the angle is, the less heat reaches those areas (Harris, 2018).

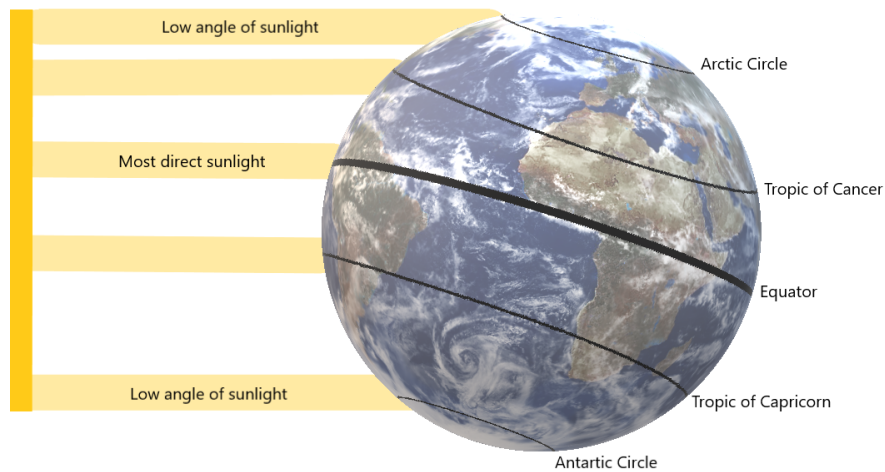


Figure 3. Sunray intensity based on Earth's location (Harris, 2018).

Unless there are perfect conditions with no weather or human interference, the path from the solar intensity from the sun to Earth can be scattered, absorbed, and reflected by many variables such as air molecules, water vapor, clouds, dust, pollutants, forest fires, or ash from volcanoes. Atmospheric conditions can affect solar intensity by as little as 10% on clear or dry days and as high as 100% on cloudy days. The more obstacles there are, the longer the distance created between the sun to the area of interest; therefore, a decrease in the sun rays' intensity (Tycorun, 2022).

For this project, we used solar data collected by the National Renewable Energy Laboratory (NREL). NREL is a national laboratory of the U.S. Department of Energy that carries out research in many energy sectors, including energy efficiency and energy systems integration. In this report, we utilized a data tool related to Energy Systems Integration and Grid Modernization, including the Solar Position and Intensity tool (SOLPOS) and Solar Position Algorithm (SPA). The SOLPOS tool calculates the maximum theoretical intensity using an algorithm that incorporates date, time, and location on Earth (NREL, n.d.). The SPA tool calculates the solar zenith and azimuth angles using an algorithm that can output values over 8,000 years (Afshin & Reda, n.d.). The calculations are based on date, time, and location on Earth and have an uncertainty of +/- 0.0003 degrees.

2.4 Solar Transmissivity

When inbound solar radiation reaches the glass on the outside of the concrete wall, a portion of the irradiation is reflected away from the glass, with the rest transmitted through it. The

fraction of transmitted energy between two mediums can be calculated based on the indices of refraction of the incident and transmitting medium, the incident angle, and the transmitted angle. The transmitted angle can be found via manipulation of Snell's Law (Nave, n.d.-b):

$$\frac{n_1}{n_2} = \frac{\sin\theta_2}{\sin\theta_1} \quad (11)$$

Where n_1 and n_2 are the indices of refraction of the incident and transmitting medium respectively, and θ_1 and θ_2 are the incident and transmitted angles respectively.

The indices of refraction and angles of light are used with Fresnel's Equations to calculate the fraction of transmitted energy from the incident beam with the following intermediate equations (Nave, n.d.-a):

$$t_{\parallel} = (2\sin\theta_2\cos\theta_1)/(\sin(\theta_1 + \theta_2) * \cos(\theta_1 - \theta_2)) \quad (12)$$

$$t_{perp} = (2\sin\theta_2\cos\theta_1)/(\sin(\theta_1 + \theta_2)) \quad (13)$$

Where t_{\parallel} and t_{perp} are the fractional transmission amplitudes in the parallel and perpendicular directions. The square of these amplitudes is the fractional transmission intensity in parallel or perpendicular directions, respectively. However, since the fractional intensities are per unit area and the area of the transmitted beam changes relative to the incident beam, these factors must be corrected to attain the fraction of the incoming energy. These transmitted energy fractions (τ) can be calculated in each direction as follows (Nave, n.d.-a):

$$\tau = t^2 * (n_2\cos\theta_2)/(n_1\cos\theta_1) \quad (14)$$

Since solar radiation has not been polarized in either direction, the net transmitted energy fraction (τ_{net}) can be calculated with the following equation:

$$\tau_{net} = (\tau_{\parallel} + \tau_{perp})/2 \quad (15)$$

2.5 Thermal Properties of Phase Change Materials

A key component of this project is material selection. Phase change materials can absorb and release thermal energy during the changing of phases. Generally, the transition is from solid to liquid, but other states of matter can also transition. Gels are also considered PCM. Due to their high energy storage ability in a compact form, PCMs have shown usefulness in storing solar thermal energy for seasonal and short-term applications (Kahwaji & White, 2021). As a result of this property, this material is pertinent to the objective. There are a variety of phase change materials, but the most common one is water. Many have experienced this phase change material, having seen solid ice cubes turn into liquid water. There are many applications of PCMs in various industries, including “solar cooling and solar power plants, photovoltaic electricity systems, the space industry, waste heat recovery systems, preservation of food and pharmaceutical products,

and domestic hot water” (Mhadhbi, 2018). Water and gel packs, salt hydrates, and paraffin are some commonly used PCMs for this work.

This project focuses on thermal energy storage for solar applications. In 1982, Solar Energy Research Institute, which later became National Renewable Energy Laboratory (NREL), completed research on solid-to-solid phase-change materials, specifically, “hydrocarbon molecular crystals were evaluated for possible use as thermal energy storage media in passive solar architectural applications” (Benson et al., 1985). Through computer simulations, they found that a Trombe wall, consisting of an ideal solid-state phase-change material could outperform a concrete Trombe wall that was four times thicker and nine times heavier; however, a setback to a PCM wall is its higher cost (Benson et al., 1985). Although PCM does have its economic setbacks, an advantage of it is its modularity, allowing it to be used where massive structures are unsuitable. Further studies have been done to incorporate PCM into concrete mixes. A two-year study was completed, monitoring results from passive solar energy storage in test cabins with phase change materials (Cellat et al., 2020). In this study, thermally enhanced concrete mixes were developed using a novel microencapsulated PCM, which resulted in daytime heat absorption from solar energy and heat released during cooler night temperatures (Cellat et al., 2020). As can be seen, there are advantages to using PCMs in construction materials to lower peak loads, reduce energy consumption for heating and cooling, and achieve reduced temperature variations, making them a viable candidate for this project.

3. METHODOLOGY

This project focuses on increasing the wall energy storage capacity of structural materials with the incorporation of phase-change materials for solar use applications in Santa Fe, NM. The following tasks guided our teams:

- Understanding solar intensity
- Development of kinetics of solar radiation
- Exploration of materials and containment
- Determining heat capacity of bricks
- Development of thermal dynamic simulation using SolidWorks

Below, we describe our approach to each task in greater depth.

3.1 Understanding Solar Intensity

NREL's website contained a database collection known as National Solar Radiation Database (NSRDB) that allowed us to obtain data from a specific point on earth, our focus point being Santa Fe, New Mexico. The data downloaded consisted of the research coordinates, latitude 35.69 and longitude -105.95, along with clear-sky DNI, clear-sky DHI, and clear-sky GHI measurements recorded every 30 minutes for the entirety of 2021 (*NSRDB*, n.d.).

DNI is Direct Normal Irradiance which refers to the direct radiation from the sun to a focused point on Earth with no interference from clouds or other atmospheric particles, creating the strongest form of solar intensity in the area of interest (Singh, 2020). GHI stands for Global Horizontal Irradiance and is the total amount of shortwave radiation that reaches the ground horizontally. These measurements are most important in determining the Photovoltaic (PV) energy that turns light into electricity. DHI represents the direct sunlight that has been diffused through clouds or reflected off the ground, causing a less intense sun ray to hit the area of interest. GHI is mathematically calculated using DNI and DHI in the following equation.

$$\text{GHI}=\text{DNI}*\cos(\text{zenith angle}) + \text{DHI} \quad (16)$$

The units for all these measurements are Watts per square meter (Singh, 2020). Our interests were solely on the DNI and DHI measurements because we needed to better understand the sun's maximum and minimum strength during the day based on the angle of where the sun would be hitting our area of interest throughout the day. Using both the DNI and DHI measurements provided us with both direct sunlight with no interference and sunlight that was diffused or reflected onto our area of interest.

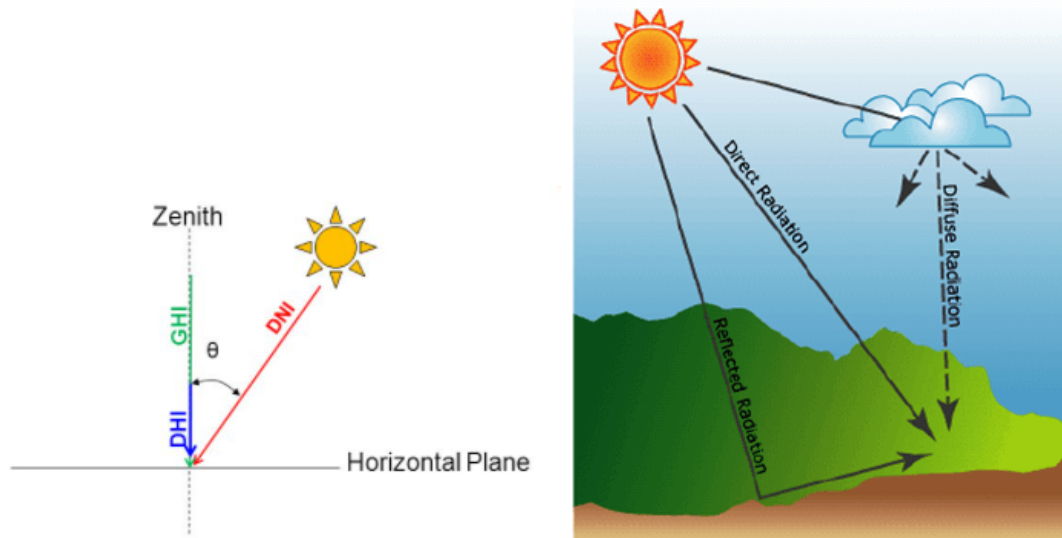


Figure 4. Solar rays with respect to DNI, GHI and DHI (Singh, 2020).

We placed the data from the NSRDB into a spreadsheet and split it up by month, including date, time, clearsky DHI, and clearsky DNI data. With data sorted by month, we went through the solar data of each day and noted the maximum clearsky DHI and maximum clearsky DNI per day. After the maximum value per day was found, they were compiled into a separate table. An example of this process is shown in Appendix A. We used this information to determine the maximum value and minimum value for both DHI and DNI within each month, as well as the date that corresponded with it. For those days we graphed the data, with the time along the x-axis, graphing only the hours in the day where the solar data recorded was greater than 0. and the solar irradiance along the y-axis. Each month had four graphs, one each for maximum DHI, minimum DHI, maximum DNI, and minimum DNI. We then added a 4th degree polynomial trendline.

Both the minimum and maximum equations for each irradiance type were taken and averaged for each month within the MATLAB tool discussed in section 3.2.

3.2 Development of Kinetics of Solar Radiation

To model the thermal response of the phase change wall, the heat flux reaching the wall was modeled over time. For a given intensity of solar radiation, the amount of radiation that reaches the wall is dependent on the transmission of the radiation through the glass wall on the outside of the wall. Since transmission through a transparent medium depends on the incident angle of radiation as described in section 2.4, we needed to create a tool to find the angle of incidence at a desired time.

As described in sections 2.1 and 2.2 the position of the sun and the angle of incidence to a wall of a certain orientation can be determined with extensively researched equations. These angles can then be used in the equations in section 2.4 to find the percentage of inbound solar radiation that is transmitted through the glass.

To allow data to be generated for different locations, different times of the year, different glass materials, and different wall orientations, these equations were used to create a tool in MATLAB that, with the addition of solar intensity modeling described in section 2.3, generates data of flux by time which can be input to the thermal simulation. This code is found in Appendix F. The MATLAB tool uses the following parameters as inputs: longitude, latitude, time zone difference from UTC, the tilt and azimuth of the wall, the start/end date, time, and the number of data points to generate data for, and the refractive index of air and glass.

This project considered a vertical southward facing wall with no shading or obstruction of sunlight. The refractive index of air is known as 1.0003. The index of glass varies over wavelength, from approximately 1.5 and 1.54 (Ulizio, 2015). While some applications may require breaking up solar radiation into wavelength bands and using an applicable refractive index in each band to calculate transmission, for this range of refractive index, the transmission varies only by less than 1%. Due to the small variance, we used an average refractive index of 1.52, which is commonly reported as the refractive index of glass. Transmission through the glass was handled in two different ways, as two different kinds of Solar Irradiance were considered: Direct Normal Irradiance, and Diffuse Horizontal Irradiance. For Direct Normal Irradiance the transmittance was calculated for each angle of incidence of the sun at a certain time following the Equations in section 2.4. For Diffuse Horizontal Irradiance, a hemispherical transmissivity was found by performing a step integral with increments of one degree and dividing the sum by 90, to find the average transmissivity over all incident angles.

3.3 Exploration of Materials and Containment

Our third task was to explore various materials for solar energy usage and storage. We combed through university databases, studied Chemistry handbooks, and discussed with local Professors to research plausible materials. In doing so, we created a property guideline for materials to help narrow down our search with advice from Professor Kmiolek, the Chemical Engineering advisor for our project. Properties considered included melting point, toxicity, and various thermal properties. We determined that the material should have a melting point between 30 and 40 degrees Celsius, slightly higher than the average temperatures in Santa Fe. An ideal material would be nontoxic and nonhazardous, as this will be used in close proximity to humans. The goal was to maximize thermal properties, such as latent heat and heat capacity, within the other specifications.

Our initial plan consisted of the implementation of phase change material within our bricks. We determined that a water-based gel material was an affordable and convenient option. Specifically, the gel that is used for hot/cold packs that are easily accessible at a local pharmacy and can be purchased in bulk from suppliers. They are mainly composed of propylene glycol, cellulose, silica gel, and water (Xin & Lyu, 2023). These gels have a high heat capacity and are non-toxic, making them a great fit for our application. Additionally, there is no volume change throughout the process of its phase change, which simplifies the design of containment within the brick. Upon acquiring the water-based gel pack, a clay pack was also bought to compare its thermal properties. They are used in the same application as water-based gels, for pain relief.

While the water-based gel packs contain the ingredients mentioned above, clay packs use a mix of ceramic clay and non-toxic oils, allowing them to maintain their temperatures for a long time (Caridad et al., 2014). However, because of their denser nature, it takes longer for them to heat up and cool down. It also has the potential to dry out when overheated or subjected to direct heat or sunlight. Although these can be seen as negative attributes for clay-based packs, we aimed to experiment with a variety of affordable and readily attainable materials. Once these materials were determined, we considered containment options.

The two factors that were most important for containment material choice were thermal conductivity and cost. Metal piping made of either carbon or stainless steel was considered due to its thermal conductivity, which is about 45 W/mK and 15 W/mK, respectively (Engineering Toolbox, 2005). These metals, however, are corrosive, which is important to consider with our gel material which is largely composed of water. Since these bricks will be used in residential construction, the corrosivity of the material was important to consider. Another option considered is plastic tubing, specifically polyvinyl chloride (PVC), which is cheaper than metal and does not corrode. The insulating properties of PVC were important to consider, as the thermal conductivity is 0.19 W/mK (Engineering Toolbox, 2011). In general, plastics are poor heat conductors because they do not have many free electrons available for conduction. To offset the low thermal conductivity of PVC, we aimed to minimize thickness, opting for thin-walled piping. We acquired various tubing options, detailed below in Table 1.

Table 1. Rigid PVC Tubing Specifications.

Inner Diameter (mm)	Outer Diameter (mm)	Wall Thickness (mm)
9.0	10.0	0.50
12.0	13.0	0.50
15.0	16.0	0.50
18.0	20.0	1.00

The structural material we decided upon was concrete. During the initial discussion about the format of our building component, we considered cinder blocks and bricks. There was potential in setting the phase change material in the existing open spaces of a cinder block or a modular brick. This was contemplated because of convenience; however, after further research and deliberation, we chose to cast our own modular blocks with concrete. Although this approach can be considered inefficient and time-consuming, it allows for the customization of PCM placement throughout each brick. The materials were purchased from a local hardware store for our concrete recipe: 2 parts Portland cement, 1 part gravel, 2 parts sand, and 1 part water.

3.4 Determining Heat Capacity of the Bricks

Our fourth objective was to determine the heat capacities of the composite material: concrete, gel, and thin-walled PVC containment. First, we cast bricks and then tested each in a

calorimeter-like apparatus. The casting of bricks was the first step in our process. We built a mold out of wood pieces — the design of which can be seen in Appendix C. The mold was coated with a thin layer of vegetable oil to allow for the easy release of the cured bricks. As discussed in section 3.3, the ratios we used for the concrete were as follows: 2 parts Portland cement, 1 part gravel, 2 parts sand, and 1 part water. This recipe allowed for the casting of three bricks at a time. If the brick had our material contained in PVC tubing, $\frac{1}{2}$ " wire fencing was used to hold the tubes to ensure they remained upright and in the correct orientation. After pouring the concrete, our bricks were left in the mold for 48 hours, then removed and left for another 48 hours to completely cure. Each brick, as seen in Figure 5, had the dimensions of 8" by $2\frac{1}{4}$ " by $3\frac{5}{8}$ ".

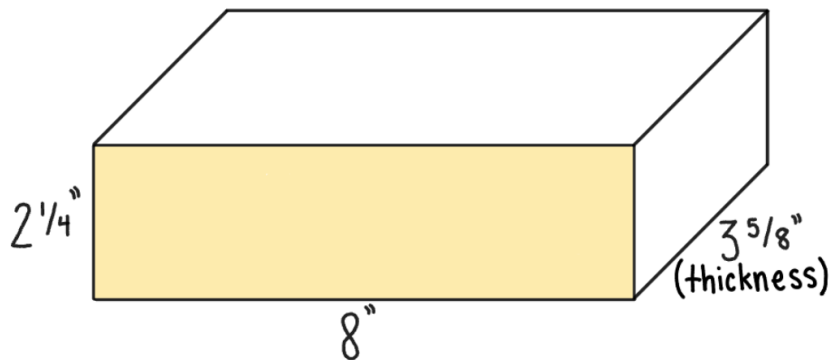


Figure 5. Schematic of brick dimensions where the face highlighted in yellow is the face exposed to sunlight, and the thickness of the thermal mass is $3\frac{5}{8}$ ".

We carried out two sets of trials. The goal of the first set was to determine the better material: gel-based or clay. Three bricks were cast. One was a control, consisting of 100% concrete with no tubing included. The other two had 2 cm OD PVC tubing filled with either gel or clay material, shown in Figure 6a. Overall, these bricks had a material volume percentage of 6%. The next set of trials used one material, determined by the previous trial, at around 6% volume and varied tubing outer diameters of 1.0 cm, 1.3 cm, and 1.6 cm. The configuration of this can be seen below in Figure 6b. Because of the use of metal fencing to hold the tubes upright, another control was tested due to the metal's conductivity properties. This control brick consisted of just concrete and metal fencing. In total, seven bricks went through testing.

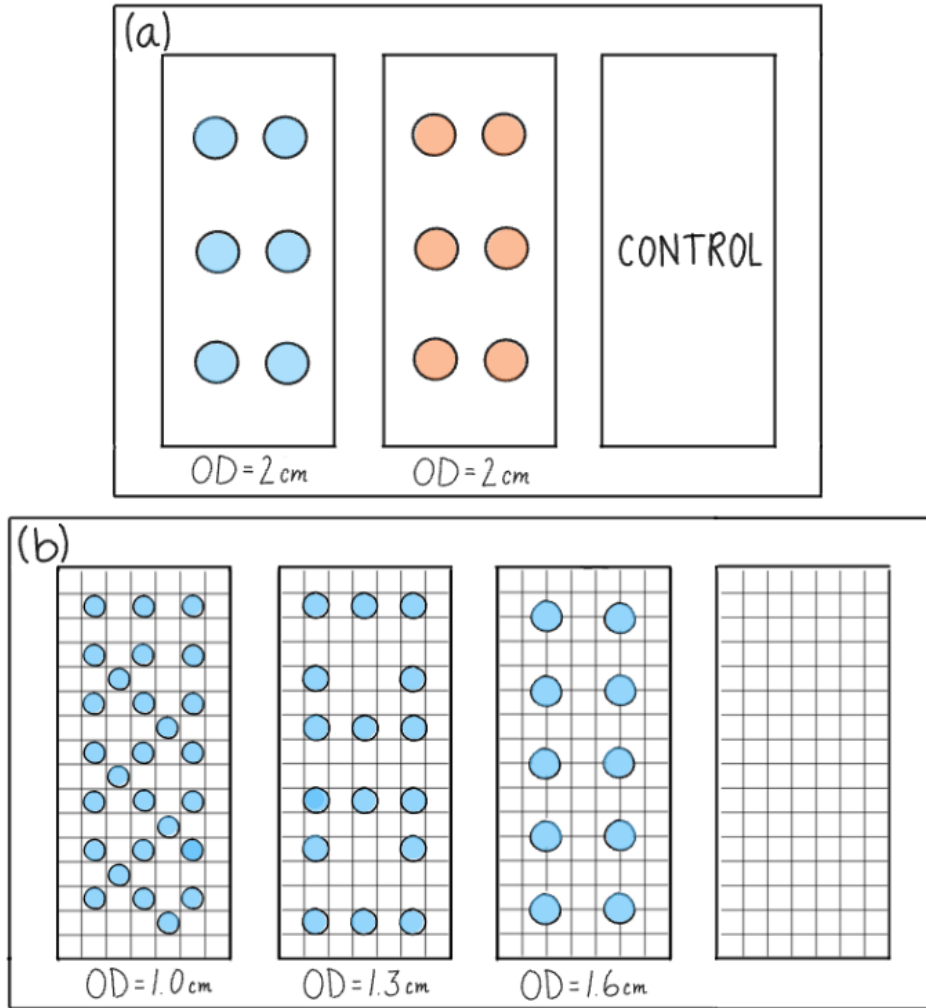


Figure 6. Tubing configurations for brick casting. (a) From left to right: Brick using gel material, clay-based material, and control brick. (b) From left to right, bricks using gel material with 3 tubing diameters and control brick with metal fencing.

To determine the heat capacity of each trial brick, we designed a calorimeter-like testing apparatus, consisting of an insulated box, metal stand, heating pad, and thermocouples to measure temperature throughout the brick. Figure 7 below shows the setup.

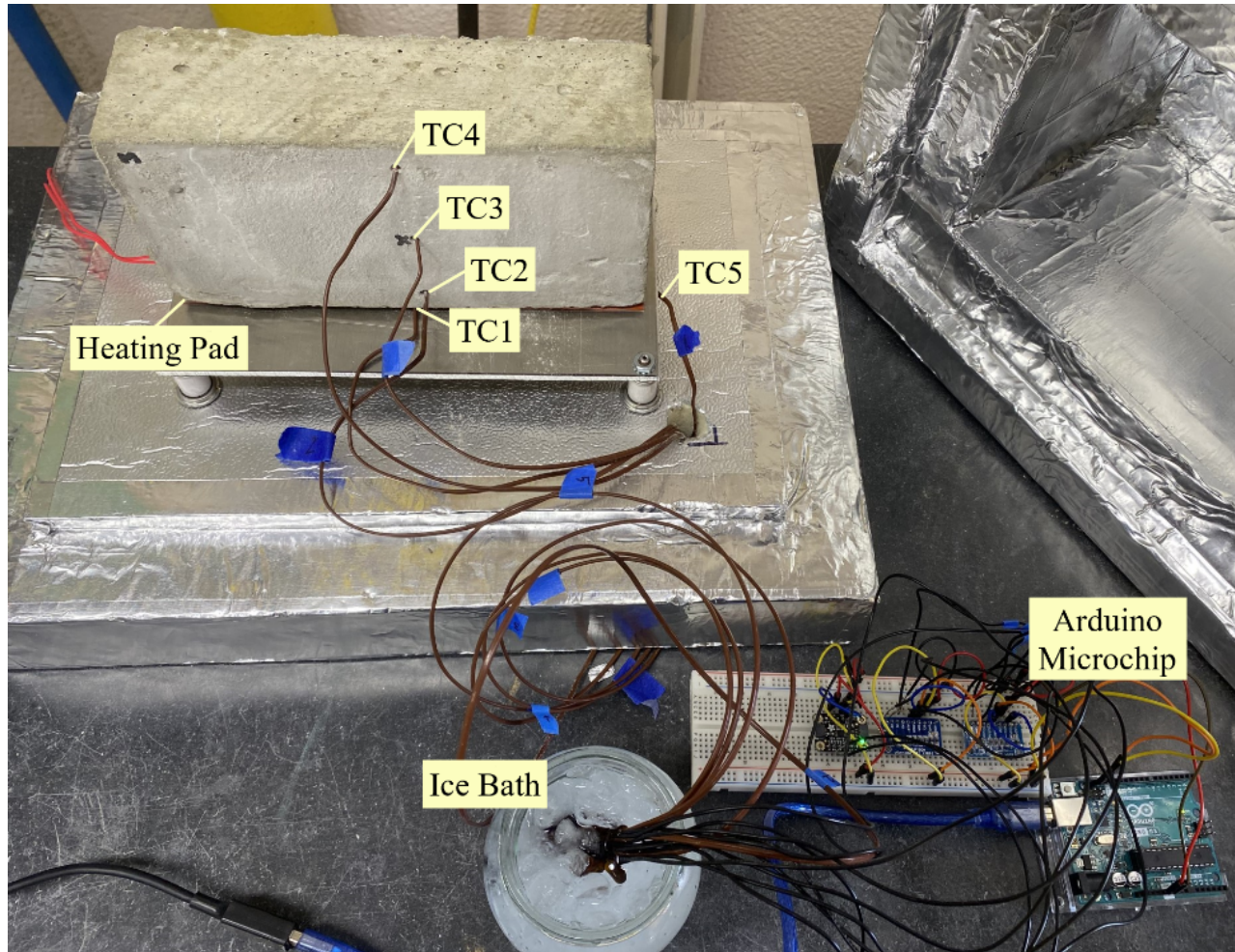


Figure 7. Brick testing apparatus with thermocouple locations noted on the brick and setup of Arduino microchip which logs temperature changes with time.

As seen in Figure 7, the 8" by 2¼" by 3⅝" brick was contained in a box constructed of R11 insulation. The insulation was 2 inches thick and wrapped and sealed with aluminum tape to reduce heat loss to the surrounding environment. The heating element used was a 160 Watt, 120 Volt silicone rubber flexible heating pad with dimensions of 2" by 8". Three ⅛" holes were drilled into each brick at ½", 1½", and 2½" from the face of the brick to be heated. A type-J thermocouple was inserted in each hole, as well as one at the heated interface and one in the ambient air of the box. The thermocouples were all connected to an Arduino microcontroller, which logged data throughout each trial at one-second intervals, as seen in Appendix D1.

In each trial, a brick was placed on top of the heating pad inside the insulated box. The power source supplied about 30 volts, corresponding to a temperature of about 35°C. A calibration curve, relating the power source input and the voltage supplied to the heating pad can be seen in Appendix D2. The time and temperature were logged throughout the process until the outermost thermocouple in the brick, located ½ inch away from the edge, reached 25°C. For a more detailed procedure, see Appendix D3.

The heat capacity of a material or composite was calculated using an energy balance around the system. The energy balance for this system is as follows:

$$Q_H = Q_{air} + Q_{brick} + Q_i + Q_m \quad (17)$$

Where Q_H is the heat supplied by the heating pad, Q_{air} is the heat lost to the air, Q_{brick} is the heat absorbed by the brick, Q_i is the heat lost to the insulation, and Q_m is the heat absorbed by the metal stand in the testing apparatus. Before starting each trial, we let the heating pad sit on the metal stand until the metal was the same temperature as the heating pad, so Q_m is assumed to be zero throughout our calculations. The amount of heat gained or lost can be modeled by the following equations:

$$Q = mc_p \Delta T \quad (18)$$

$$Q = UA\Delta T_{LM} \quad (19)$$

Where m is mass, c_p is heat capacity, ΔT is the temperature difference, U is the overall heat transfer coefficient, A is surface area, and ΔT_{LM} is the log mean temperature difference between the ambient air and air inside the chamber. The following equation shows the energy balance with Equations 18 and 19 substituted where necessary.

$$Q_H = m_{air} c_{p,air} \Delta T + m_{brick} c_{p,brick} \Delta T + U_i A \Delta T_{LM} t \quad (20)$$

This equation can be solved for the heat capacity of the brick, $c_{p,brick}$, for each trial. Sample calculations can be seen in Appendix E.

3.5 Development of Thermal Simulation using SolidWorks

Data on the solar flux transmitted through the glass wall generated from our MATLAB tool, heat capacity, density, and thermal conductivity of the bricks were input into SOLIDWORKS as incident heat flux to the wall and material properties, respectively. Using these data sources, thermal simulations were run for the first day of each month in each configuration, to evaluate the thermal cycle of different bricks relative to each other. Each heat flux time curve began at 3:00 AM on the first of the month, went until 3:00 AM on the second day of the month, and contained 201 data points. The SOLIDWORKS simulations were run as transient simulations over the full 24 hours of the input data at 1,000-second time steps. The simulations used an initial temperature of 71°F, boundary conditions of convection, and radiation on both sides of the brick, assuming the ambient temperatures of the room were held constant at 71°F. A convection coefficient of 10 W/m²K, typical for free convection of air, an emissivity of 0.9, and a view factor of 1.0 were used (MPA, n.d.).

The time curves for each month were examined to find the approximate inflection point after the peak of the sun's intensity for the day. An example time curve is shown below in Figure 8. The energy released from each brick configuration after this time until the end of the dataset was found from the results of the thermal simulation. These results were compared from brick to brick

within each month to find the percent increase of energy released after the sun's intensity waned, the time in which Trombe walls passively heat a space. This enabled us to determine how much more effective the bricks containing phase change material were compared to a standard brick wall.

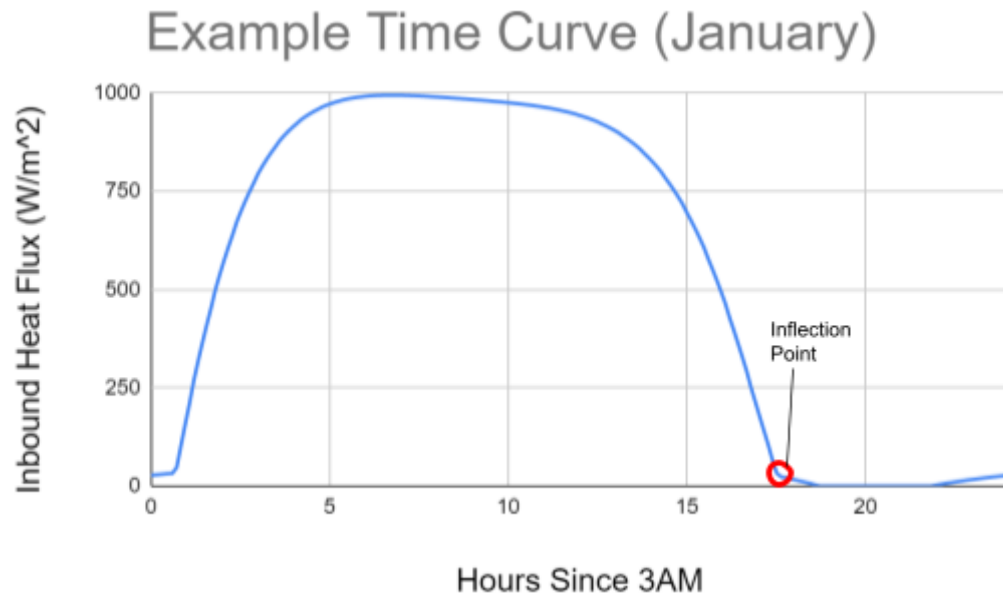


Figure 8. An example time curve of inbound heat flux for January, showing the inflection point used to determine the start of the time range energy released was compared over.

4. RESULTS and DISCUSSION

The main goals of our project were to compare bricks incorporating phase-change material to standard Trombe wall concrete bricks. To make this comparison we developed a tool to model solar behavior in Santa Fe, selected a material to increase passive solar capture, and combined these aspects to create a thermal simulation of our wall in New Mexico.

4.1 Heat Capacity of Bricks

Heat capacity is the amount of heat required to raise an object's temperature by one degree, indicating a material's ability to absorb heat. With a higher heat capacity, a house wall can more efficiently take in heat to reduce the use of external heating devices. As mentioned in sections 3.3 and 3.4, seven different bricks were tested using the calorimeter-like testing apparatus, and the heat capacity of each was calculated.

Our first set of trials aimed to determine which material, gel or clay, would have a higher heat capacity. The control brick took 14.23 minutes to heat one degree from 23°C to 24°C; the clay-containing brick took 13.88 minutes, and the gel-containing brick took 13.02 minutes. The gel brick took the least amount of time to heat up, suggesting that the heat capacity will be larger as well. Table 2 below details the calculated heat capacity for each trial as well as the percent increase compared to the control.

Table 2. Heat Capacity for Bricks with Different Materials.

Brick	Heat Capacity (kJ/kg K)	% Increase
Control	1.198	-
Clay Material	1.281	6.97
Gel Material	1.295	8.15

The gel-containing brick had a higher heat capacity than the clay brick with an additional 2% increase from the control. Once we determined that the gel provides a higher heat capacity, we carried out another set of trials with only the gel to determine the PVC tubing diameter that maximizes the composite brick's heat capacity. Figure 9 below displays the results for our small, medium, and large diameters compared to the control.

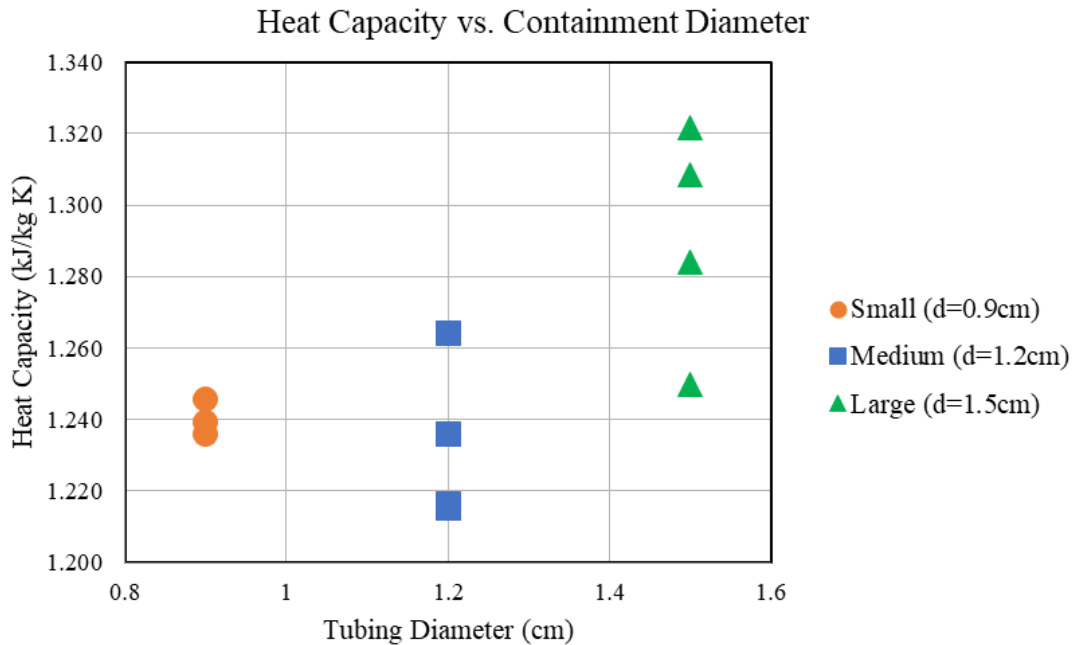


Figure 9. Calculated heat capacity of composite brick based on containment diameter.

The largest tubing diameter, 1.5 cm, resulted in the largest heat capacities of the composite brick. This deviated from initial expectations. The smallest diameter had the largest surface area contact with the concrete, which we hypothesized would lead to a quicker rate of heat transfer between the material and concrete. While this may have been true, the rate of heat transfer from the warmed gel to the colder side of the concrete would be increased as well. Results indicated that the largest diameter allowed the gel to hold heat better. Four trials were conducted for each tubing size, and the average heat capacity values throughout the trials, along with the percent increase of heat capacity compared to the control brick are detailed in Table 3.

Table 3. Average heat capacity of composite bricks, depending on tubing containment diameter.

Brick	Brick Heat Capacity (kJ/kg K)	% Increase of Heat Capacity
Control	1.190	---
Small (0.9cm) Tubing	1.240	4.207
Medium (1.2cm) Tubing	1.233	3.587
Large (1.5cm) Tubing	1.291	8.472

As seen above in Figure 9 and Table 3, the medium-sized tubing deviated from expected trends. In general, the experimental results for heat capacity were lower than expected and on average had the smallest increase in heat capacity compared to the control. There are several

reasons that this may have happened. First, we wrapped some thermocouples in aluminum foil to increase contact between the thermocouple and concrete surface. This was not done consistently and may have caused some deviation in data collection between bricks. Also, the Arduino code for the thermocouples was based on a zero-degree reference. Although we cycled new ice through the ice bath, at times the reference may have been higher than anticipated leading to erroneous temperature readings at times. Aside from data collection, the testing apparatus was not perfectly sealed, so the calculation for heat lost to the environment was likely slightly larger than calculated. Additionally, energy from the heating pad was first absorbed by the metal stand that the brick rested on. To combat this, we allowed the metal stand to come to thermal equilibrium with the heating pad before placing the brick in the apparatus. However, if the metal and heating pad were not at the same temperature, heat would be absorbed into the stand and not the brick. Our calculations assumed that the heat absorbed by the metal stand was zero at the start of each trial. If this was not true in practice, our values for heat capacity could be erroneously high. Nonetheless, a consistent procedure was used for each trial, so the comparison between control and test bricks is valid.

4.2 Solar Intensity Modeling

The data of maximum and minimum DHI and DNI within each month were compiled to create a total of 48 graphs. The graphs for months January and June are shown in Appendix B. A trendline for each graph was fit to a 4th degree polynomial which estimated the measured DNI or DHI for each hour. The equations for each month, as well as their R^2 values are tabulated in Appendix B. The R^2 value for each of the trendlines ranged between 0.981 to 0.9997 throughout the graphs, with no significant trends between months. These high R^2 values indicate a good fit of the data, making our estimates of maximum and minimum DNI and DHI highly accurate. The importance of the equations found through this process is to use them as a range of where the DNI and DHI would be for each month. The range of values are used in the thermal simulation of our brick, to measure the useful passive energy released.

4.3 Thermal Simulation/Cycle

The thermal simulations of the brick found increases in useful passive energy release ranging from 4.74% to 9.55% for the different PCM brick configurations. The percent increases for each brick are shown in Table 4. This table shows that the Large Tube PCM bricks performed the best and that the Medium Tube PCM Bricks performed the worst out of the bricks containing phase change material. However, all phase change material containing bricks simulated performed better than a standard Trombe wall brick. Tables with the generated data used to calculate these percent increases are found in Appendix G.

Table 4. The table displaying the relative increase of energy released for PCM bricks compared to a standard Trombe wall brick.

Brick Type	Average Percent Increase of Energy Leaving the Brick Between "sunset" and 3 AM Compared to Control Brick
Small Tube PCM Bricks	4.74%
Medium Tube PCM Bricks	4.08%
Large Tube PCM Bricks	9.55%

Other outputs from the thermal simulation are displayed in Figure 10. This figure shows how the brick absorbs energy at the beginning of the day and begins to release more energy than it absorbs as the day progresses. This graph also demonstrates the principles of passive solar systems, showing how during the day energy flows into the brick, and later in the day flows out of the brick.

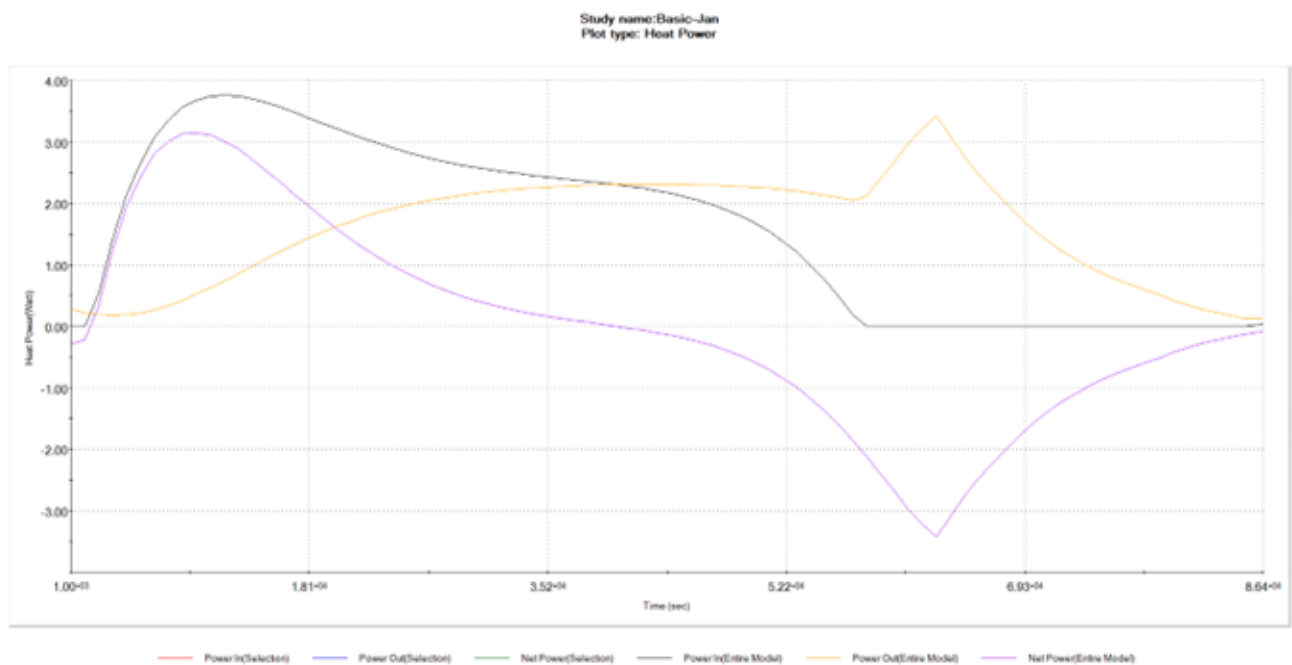


Figure 10. A chart showing the variation in energy in and out of the brick for a standard Trombe wall brick simulated in January.

4.4 Cost Analysis

To look at the possibility of this brick being applied in the building industry, we did a basic cost analysis for the materials required and the energy savings that this could provide. The bricks consisted of Portland cement, gravel, and fine sand to form the main component cement and also

included gel material, thin-walled PVC tubing, and metal fencing for structural purposes. The total price per brick was \$2.35. All costs were based on our purchase price from retailers such as Home Depot and CVS. If the bricks were produced on a larger scale, this cost would be significantly reduced as our materials would be purchased for wholesale prices. An estimation, assuming a markup percentage of 15% from wholesale to retail results in the cost per brick to be reduced to \$2.00. This is compared to a typical cost per brick of \$0.98 at a hardware store (Lowe's, 2023). While our material costs for the bricks are about double the standard modular brick cost, the energy savings that result in the years following construction will benefit customers. Additionally, these costs do not include consideration of any added manufacturing costs such as labor.

For our heat flux analysis, we based the Trombe wall assembly on the design of the Trombe wall at the Zion National Park Visitor Center featured in a 2004 NREL study. The NREL found through performance testing of the building that the wall contributed 20% to the total heating needs of the building (NREL, 2004). It is difficult to determine the exact energy savings that our modified bricks would provide without a complete building layout and architectural energy modeling, but assuming that the Trombe wall in Zion is comparable to the thermal qualities of our solid cast concrete brick, we can estimate a 9.55% increase in energy release into the space after sunset, corresponding to an estimated 22% reduction in heating costs for a comparable space. It is difficult to translate this reduction into a monetary amount due to the variability of heating costs and performance with different homes.

4.5 Limitations

There were three main parts to our results: heat capacity, modeling solar intensity, and full thermal simulation. In testing, our team experienced supply chain issues which ultimately led to time constraints during the testing process. The vendor for the thin-walled PVC tubing we used was a Chinese company Harfington, and the material took about two months to arrive. This vendor was one of the few we researched that had tubing in our desired diameters and thickness. With more research into vendors, a more efficient vendor with readily available tubing could be identified. These supply chain issues for sufficient containment of our material led to our inability to test different amounts of material throughout the brick. Each trial maintained a consistent volume percentage of the gel material between 6-7 percent. Our calculations for the volume percentage of empty space in the holes of a standard modular brick was 15%, so we knew that was our limit to maintain structural integrity. If we had access to more time for additional tubing to be ordered, we could have increased this percentage up to 15%, which would likely correspond to an even higher heat capacity of the composite brick. Even further testing could potentially increase the volume percentage past 15%, but this would require analysis of architectural loads and structural integrity to ensure that a wall would still be suitably strong even with less concrete than a standard brick.

Next, we focused on modeling solar intensity with NSRDB data specific to Santa Fe, New Mexico. The output of the increased heat produced per brick would vary based on location in relation to the location, with warmer climates having a higher success rate compared to colder regions. Another factor would be the type of geographical living area, where rural/suburban areas

have a better outcome compared to urban areas due to the structure of the buildings. The weather is another major factor in the solar intensity. Since we used data specific to the year 2021, the range of values for DNI and DHI might differ in the coming years due to the uncertainty of temperature changes, solar intensity changes or an increase/decrease in other weather conditions such as rainy, snowy or cloudy days. The change in DNI and DHI values will affect the range of values inputted into the thermal simulation, creating a different percentage for the useful heat produced for each brick.

There were several limitations associated with the thermal simulation of PCM bricks. Because the energy released was analyzed from a post-intensity peak inflection point until 3:00 AM for every month, the actual amount of energy released cannot be compared between months. As the solar intensity pattern is not the same from month to month, some months left out comparably more time where the sun would be down after 3:00 AM where the brick could still be releasing energy. While results cannot be compared between months, they can still be compared within a month, as the same time curve and analyzed time range was used within each month. Additionally, our thermal simulation did not take into effect variances in ambient room temperature and convection caused by energy release from the brick. It also considered the room and the hot air layer between the glass and the brick as having the same properties. This could be modeled more accurately in combination with an actual home layout and specifications, as well as varying ambient temperature conditions and home air flow details in fluid simulations to produce the actual reduction in the amount of active heating energy required for a specific setup. Such a level of simulation detail was beyond the scope of this project. This means that our simulation results cannot directly determine the reduction in active heating energy required, and are limited to comparing efficacy to standard Trombe walls. However, using external results for the performance of standard Trombe walls relative to regular walls, our results can be used to estimate how much energy such phase change material bricks in Trombe walls could save. Our simulation also did not take into account that a room may not be maintained at the same temperature for an entire day, neglecting changes in desired temperature associated with a time of day and resident's activity level.

4.6 Passive Solar Retention and Release

As described in this report, the item being tested is a modified Trombe Wall that contains phase change material (PCM) in order to store and release greater amounts of heat energy than brick or concrete could on its own. The most effective orientation of a Trombe wall is south-facing in the northern hemisphere and north-facing in the southern hemisphere. A Trombe wall is most effective in a location that is sunny year-round, and has a higher solar intensity. In this section we discuss how this technology can be applied in the context of new construction of homes, as well as retrofits. In particular, we discuss policy incentives and funding mechanisms that could enable such technology to be universally available to more people. Finally, we make two recommendations for the state of New Mexico to follow in order to spread the word about this innovative technology.

New Mexico has a long history of using passive solar. The Anasazi of New Mexico used passive heating and cooling long before its popularity in the 1970s, “as evidenced in Chaco Canyon and Mesa Verde communities of A.D. 1100” (Hunn, 2022). They made multi-family dwellings that “were built facing south to maximize the heating of the winter sun and were insulated in the north by tall walls as Chaco Canyon and Bandelier National Monument, or as a cliff dwelling, as at Mesa Verde” (Hunn, 2022). These are two of many examples of passive solar architecture developed by Indigenous Peoples in the southwest. In the two decades leading up to the 1970s, fossil fuels were cheap and widely available, reducing the usage of passive solar heating and cooling in building design. However, in the 1970s, fuel costs rose drastically, renewing the region’s interest in passive solar technology (Hunn, 2022). This included the planning of a microcity within Albuquerque, NM called Mesa del Sol. Mesa del Sol is a community that is deeply focused on being smart, sustainable, and safe. They are passionate about implementing smart infrastructure, microgrid technology, smart transportation, geodesign and solar and wind energy generation (Chavez, n.d.). Geodesign is responsible management of resources in the community while considering future impacts, which would include passive solar design.

In 2013, there was a Solar Decathlon sponsored by the U.S. Department of Energy, where Arizona State University and The University of New Mexico designed a house, called Solar Homes Adapting for Desert Equilibrium (SHADE), that prominently features phase change materials. The “phase-change material distributed throughout the house stores thermal energy and buffers temperature fluctuations by redistributing the energy as passive heating and cooling” (US Department of Energy, n.d.). After the decathlon, SHADE was moved to Mesa del Sol through March 2014, where further research could be conducted on the “smart-grid integration and the radiant/thermal storage and controls systems” (US Department of Energy, n.d.)). While it is encouraging that there is passive solar innovation in a dedicated community like Mesa del Sol, phase change materials and modified Trombe walls could be used much more broadly in the state of New Mexico and in the southwest region of the United States to help address climate change. Policy incentives and funding mechanisms could help with the spread of these technologies, as they have grown with the acknowledgement of the climate crisis and the U.S. Inflation Reduction Act. The Inflation Reduction Act (IRA) is a tax law published in the United States of America on August 16, 2022 that will help curb inflation, reduce carbon emissions, lower prescription drug prices and help Americans afford renewable and more efficient energy, vehicles, home renovations and appliances (The White House, n.d.). Next, we will discuss federal and statewide incentive programs, as well as funding strategies that could help achieve the broader use of the passive solar technologies.

4.6.1 New Builds

Policy incentives, in this case, are laws, tax credits or other policies that motivate people or companies to implement certain actions or appliances that are better for the environment, but may cost more than their inefficient alternatives (Larsen et al., 2022). For example, a standard water heater may be cheaper than a high efficiency water heater, but the high efficiency appliance is more sustainable, could last longer, and will require less energy than the standard option. By

introducing a tax credit or rebate for those who purchase the more efficient model, this motivates consumers to make the better choice. Similarly, each experimental brick that is used to create the modified Trombe wall costs about double that of a brick from a standard Trombe wall. Since the modified Trombe wall is about 10% more efficient than a standard Trombe wall, it is a more sustainable and energy saving choice. So, if we can use policy incentives to monetarily encourage homeowners to choose the modified Trombe wall instead of the standard one, it is a benefit to the homeowner and the environment.

State Level Policy Incentives

Many states in the US have programs and incentives for energy efficiency in homes, places of business, etc. An example of a state-wide incentive is the Mass Save program in Massachusetts. Mass Save is a “collaborative of Massachusetts electric and natural gas utilities and energy efficiency service providers” that help “residents, businesses and communities to make energy efficient upgrades by offering a wide range of services, rebates, incentives, trainings, and information” (Mass Save, n.d.-a). Currently, Mass Save is offering Residential New Home Construction Incentives for single-family homes and multi-family homes that are 3 stories or less. These incentives are intended to encourage and financially assist homeowners to build high-performance, energy-efficient homes that exceed the Massachusetts building energy code. There are even enhanced incentives for homes that meet certain high-performance, all-electric criteria. Incentives through this program are determined and calculated based on the amount of electric savings, fuel savings and overall performance when compared to the average new home in Massachusetts (Mass Save, n.d.-c). Participants of this program not only get rebates and financial incentives by building energy-efficient houses, but they end up paying less for energy in the long run.

This program could easily expand to accommodate the modified Trombe wall referenced in this report. Since the modified Trombe wall would help reduce the amount of energy needed to heat and cool a home, it should count as energy-efficient building material under the Mass Save guidelines. When taking a closer look at the features required for a home to qualify under this program, one of the features is “efficient heating and cooling equipment” (Mass Save, n.d.-b). While a structural wall may not be considered as equipment, we believe that it satisfies the same intention of increasing efficiency and decreasing the amount of energy needed for heating and cooling. By adding Trombe walls as an option to the Mass Save program, it could be utilized more often and to its full potential. It should be noted that Massachusetts is not the ideal location or climate to implement the use of Trombe walls, however, it is a fitting example to show how easily it would be to include the Trombe wall into the language of incentive programs like this in order to incentivize their use.

The State of New Mexico has an Energy Conservation and Management Division (ECMD) that helps move the state towards clean energy adoption. According to the state government website, “ECMD is committed to developing the deploying solutions that will maximize New Mexico’s renewable energy resources and improve energy efficiency and transportation standards” (New Mexico Energy, Materials and Natural Resources Department, n.d.-a). The ECMD website

details the programs available, including their tax credit program that highlights the Sustainable Building Tax Credit. When looking closer at the Sustainable Building Tax Credit, there are two types of credits underneath this program: one for existing residences and another for commercial renovations or new construction. The ECMD also provides a list of qualifying items and services that count for this tax credit: Energy Star air source heat pump, Energy Star ground source heat pump, Energy Star windows and doors, Insulation improvements that meet department's rules, Energy Star heat pump water heaters, and/or Electric vehicle ready (New Mexico Energy, Materials and Natural Resources Department, n.d.-b). As will be addressed later in the recommendations section, the modified Trombe wall would be an excellent addition to the Sustainable Building Tax Credit because it has similar, if not better, energy saving capabilities than appliances and renovations already approved for use through the program.

Green Banks as Funding Mechanisms

Creating policy incentives is a good start to encouraging families and businesses to incorporate Trombe walls, renewable energy or energy efficient additions, but there is a need for larger and more long term funding for these climate-friendly solutions. With the creation of the U.S. Inflation Reduction Act came \$20 billion in funding from the Federal Government to green banks all around the country. Green banks are “specialized banks that lend money to homeowners and businesses for energy-saving and climate projects” (Brown, 2023). Green banks provide loans that are typically longer-term and lower-interest alternatives to typical banks, and many focus their work in low- to moderate-income communities that have the greatest need for energy upgrades and the least access to funding. A big incentive for residents and businesses to take advantage of green bank loans is first the ability to lower energy costs and second to help put local contractors to work (Brown, 2023). Some communities have already seen success in the usage of green banks. For example, the Hawaii Green Infrastructure Authority “has helped residents install rooftop solar panels”, allowing them to shrink utility bills as energy costs rise, as well as creating a program “to allow renters to pay for energy upgrades with a charge on their utility accounts” (Brown, 2023). Giving families and businesses access to these loans gives them the autonomy to make climate-conscious decisions with less concern of being able to afford such things. This gives more access to low- and moderate-income families to afford changes that will save them money and help the environment in the long run. Green banks can help fund the implementation of modified Trombe walls into new houses, as they would be considered a sustainable or environmentally friendly addition to your home.

4.6.2 Retrofits

The modified Trombe wall, as discussed throughout this report, is more effective than a standard Trombe wall, and works best in new builds or major renovations to an existing building. However, since so many of the homes and infrastructure in the United States are already built, retrofitting these buildings is crucial to achieving energy efficiency, rather than demolishing old buildings and replacing them with new ones. So, how do we incentivize retrofitting? First, let's look at ways in which a modified Trombe wall can be utilized in a retrofit context.

Case Study of Retrofits for PCM

As stated before, the modified Trombe wall works best in residential new builds. Therefore, when looking into retrofitting existing homes, it is best to use a different method for incorporating phase change material (PCM) into housing material to achieve more energy-efficiency. There are a number of studies that explore the effectiveness of PCM in buildings. For example, one research study compared the effectiveness of a retrofit PCM panel onto the outside of a house in two different climates (Imafidon & Ting, 2023). The retrofit panel was to be attached to the exterior of an already-existing home or building to help control the amount of heat gain and loss from the building. The control study was done in Ottawa, Canada, which has a large temperature variation during the span of a year. The experimental study was done in Brasilia, Brazil, where there is very little temperature variation during the year.

The study explored the effectiveness of a retrofit panel, which consisted of exterior oriented strand board (OSB) sheathing, polystyrene insulation, and a PCM wallboard. After the panels were tested in both Canada and Brazil, it was concluded that the PCM retrofit panels were most effective in a climate in which the average ambient temperature is about the same as the desired internal temperature of the building. The study also determined that the positioning of the PCM layer within the panel mattered. The panel was most efficient when the PCM layer was on the interior of the panel, which is the same as the old exterior of the house, as opposed to in the middle or outside of the retrofit panel. After these findings were discovered, the total heat loss and heat gain savings were calculated. In Ottawa, the paneling was most effective between May and September, and the heat loss, or heating savings, during those months was 13% and the heat gain, or cooling savings, during those months was 8%. In Brasilia, the paneling was effective all year long and the heat loss was found to be 27% and the heat gain was found to be 2% (Imafidon & Ting, 2023).

Federal Policy Incentives for Retrofits

First, we will begin by talking about a federal example of incentivizing retrofits via the U.S. Inflation Reduction Act. There is one section of the Inflation Reduction Act that we will focus on: Section 179D. Prior to the IRA, the tax deductions discussed in Section 179D were somewhat exclusionary, as they were only open to owners of commercial properties or residential properties of four stories or more. Prior to the IRA, there was also a rule that the taxpayer was required to show a 50% reduction in energy and power cost. Now, the IRA expands access to this deduction in two ways. The first change is that those with buildings of 3 stories or less can now qualify for this deduction. The second change starting on January 1, 2023, is the threshold for energy savings drops from 50% to 25%. Because of these two massive changes, this opens up the credit to thousands of homeowners who previously wouldn't have qualified. This means that more people can be incentivized to make sustainable and energy-efficient changes to their houses (McOmber, 2022). Research has shown that by implementing a modified Trombe Wall into your home can reduce energy usage by around 22%. Therefore, implementing our version of the modified Trombe Wall into residential homes could help families get closer to the 25% threshold to achieve the requirements for this deduction. Though it would be necessary to incorporate more

energy-saving appliances or features to reach the minimum requirement, the Trombe Wall would be significant in meeting the energy savings requirement, while also being good for the environment by reducing carbon emissions.

Based on the analysis in the case study, we know that this type of PCM paneling would be very effective for retrofitting buildings that have a similar climate to Brasilia, Brazil. Specifically in this case, these retrofit walls seem like they could be very effective in Santa Fe, where we based our solar modeling on. Based on the 27% heat loss shown above, it appears that by adding a PCM retrofit wall, there is the possibility to hit the 25% energy reduction threshold stated above by the Inflation Reduction Act and could contribute to property owners achieving enough energy savings to use the credit. These retrofit PCM walls look to be an efficient addition to homes that may lack good insulation, as long as they are in the proper climate.

Grants as Funding Mechanisms

Another example of funding mechanisms to help homeowners pay for the, sometimes, costly updates to make their homes more energy efficient is grants, whether they be private, or government funded. Grants are monetary awards, in this case from the Federal Government, that do not need to be paid back, but are only allowed to be used on certain things designated by the grant provider (Grants.gov, n.d., p. 1). In this case, these grants could incentivize citizens to make energy efficient improvements to their homes, by paying for some or all of the upfront costs of the improvements. These grants could be expanded to include passive solar, PCM, or modified Trombe walls in the list of approved improvements. One example of a government sponsored grant is the Low Income Home Energy Assistance Program (LIHEAP). The LIHEAP “helps keep families safe and healthy through initiatives that assist families with energy costs” (Administration for Children & Families, 2023). The LIHEAP grant is federally funded and given to states, federally recognized tribes, tribal organizations, and territories. These states, tribes, and territories are then responsible for allocating the funds properly to households in need. This grant in particular is to be awarded to low income families to help reduce costs related to home energy bills, energy crises, weatherization, and minor energy-related home repairs. This kind of assistance is very important, as it helps alleviate the financial burden of upgrading home energy-efficiency to low-income households. It also allows these households to make energy upgrades that will cost them less money in the future, and helps the United States to lessen their impact on the environment.

Another grant that is provided by the U.S. Department of Energy (DOE) is the Weatherization Assistance Program (WAP). Similar to LIHEAP, WAP aims to reduce “energy costs for low-income households by increasing the energy efficiency of their homes, while ensuring health and safety” (Office of State and Community Energy Programs, n.d.-a). This grant is for low-income families, especially those that are elderly, disabled, and children. According to the DOE, “Low-income households typically spend 13.9% of their total annual income on energy costs, compared to 3.0% for other households” (Office of State and Community Energy Programs, n.d.-a). With the receipt of the WAP grant, homeowners can expect to have lower energy costs due to some or all of the following renovations: replacing appliances with energy efficient alternatives,

insulation, air sealing, new energy-efficient windows or doors, repair/replacement of venting systems, safety repairs, repair/replacement of heating and cooling systems, repair/replacement of water heaters, and many more (Office of State and Community Energy Programs, n.d.-b). WAP is comparable to LIHEAP in the way funds are received and disbursed. The DOE awards the funds to states, tribes, and territories, who in turn give the grant funds to local organizations and contractors to perform the weatherization services to low-income families. This program stimulates the local economy by improving low-income housing, reducing energy costs therefore leaving the recipients with more money to spend on other necessities and extra wants. Furthermore, local companies and contractors, in cooperation with the state government, are provided with more work, and fair compensation. Financial assistance through grants like this is a win-win situation for local contractors, low-income families, and the environment.

Educational Incentives in New Mexico

The Sustainability Education for Advanced Building (SEAB) is an energy conservation code training for professionals. The New Mexico Energy, Minerals, and Natural Resources Department has partnered with 4 local colleges, Doña Ana Community College, Northern New Mexico College, San Juan College, and Santa Fe Community College, to provide free education and training about the state energy conservation codes to construction industry professionals. They provide separate trainings for both design professionals and for plan reviewers and inspectors. The courses help professionals learn about both residential and commercial energy conservation codes, as well as the associated codes in standards. These trainings also fulfill continuing education unit (CEU) or professional development hour (PDH) requirements (New Mexico Energy, Materials and Natural Resources Department, n.d.-c). If this program could incorporate training sessions about passive solar, PCM, and modified Trombe walls, it could help to educate the professionals who would be able to advocate for the use of these energy efficient technologies.

5. CONCLUSIONS and RECOMMENDATIONS

5.1 Future Work and Applications

In future work with this project, our team recommends the exploration of how chosen experimental heat source, configuration, and volume percentage used in the bricks will affect the heat capacity and other thermal properties of the building material. During the planning stage of our testing apparatus, in conversation with chemical engineering lab technicians, multiple options for the heat source were discussed including ovens, heat cartridges, and heat lamps. Out of these options, we recommend experimentation using a heat lamp as the energy source. The radiative heat provided by a lamp could more closely mirror radiation from the sun, which may result in improved results for this application. Aside from the testing setup, variables that we did not explore were the configuration of the material and the volume percentage of the gel. As noted in our limitation section, the volume percentage was constrained by the tubing on hand. With additional experimentation and sufficient material, a higher volume percentage could be achieved. Furthermore, the configuration of the material can deviate from the modular brick we modeled. An example would include an eight-inch by eight-inch by sixteen-inch concrete block, another typical building material used in home construction. The volume percentage would again change and different containment options could be explored, which would change the energy storage capacity of the composite material.

In addition to different heat sources, material configuration, and volume percentage, assembling the final building material to mimic a Trombe wall can be examined. This would consist of simulating the conditions of a wall like painting the building material a dark color to better absorb sunlight, selecting specific glazing whether it is insulated or has low emissivity, and adjusting the space between the wall and the glass. These are all extra variables that can be changed, while others are controlled, which affects the final efficiency of the Trombe wall.

Moreover, because Trombe walls are dependent on sunlight, it is a given that as the seasons change, so does sun exposure. If an improved building material was implemented in a home it cannot be removed, so to counter the everchanging seasons extended roofs or overhangs can be used. This is important when structures will get ample direct sunlight in the summer because the shade can be provided to help keep the home cool; meanwhile, extended roofs or overhangs can also help direct sunlight to the Trombe wall to maximize heat absorption during winter. Various designs that control roof angles and lengths can be created based on home aesthetics and desired functions.

More detailed flow simulations with specific home layouts and specifications could also be performed to determine actual energy and cost savings directly. This could also more fully account for the complexities of heat transfers effect on the convection in the room and changes in desired temperature over time, as discussed in section 4.5.

While there are several areas of further research and testing, our results found that incorporating phase-change materials to a Trombe wall causes increases in useful passive solar energy. These findings can be used in home construction to further decrease the amount of active

heating required in homes, reducing annual heating costs, and the environmental impact caused by active energy consumption.

5.2 Recommendations for Policy Incentives and Funding Mechanisms

Adding modified Trombe walls, PCM, and passive solar technology to policy incentives in New Mexico could be very beneficial. Based on Energy Star's website, "replacing old windows with ENERGY STAR certified windows lowers household energy bills by an average of 12 percent nationwide" (Energy Star, n.d.-a). Traditional "water heaters use about 20% of a home's energy", but by switching to an Energy Star heat pump water heater you can use up to 14% less energy, meaning that by upgrading to the more efficient model, the water heater will only use about 6% of you total home energy (Energy Star, n.d.-b). The modified Trombe wall discussed in this paper has an estimated 22% annual energy savings. Based on these numbers, the Trombe wall is 8% - 10% more effective in saving energy than both upgraded windows or water pumps. Therefore, we believe that since the Trombe wall is within the same order of magnitude of energy savings, that it should be incorporated into the Sustainable Building Tax Credit program. This addition would serve to give homeowners more flexibility and options for upgrading their homes as well as combating climate change.

Based on the effectiveness of Trombe walls and passive solar when it comes to energy conservation, we believe that it should be added into this SEAB training. Whether it is integrated into an existing training, or a new training is created to address energy efficient building techniques, it would benefit homeowners, builders and planners to have more knowledge of their energy efficient options. With the new knowledge of the PCM, passive solar, and associated policy incentives, construction professionals are more likely to use these technologies and offer them to their customers, which saves energy.

REFERENCES

- Administration for Children & Families. (2023, January 31). *Low Income Home Energy Assistance Program (LIHEAP)*. Administration for Children & Families.
<https://www.acf.hhs.gov/ocs/low-income-home-energy-assistance-program-liheap>
- Afshin, A., & Reda, I. (n.d.). *Solar Position Algorithm (SPA)*. Retrieved March 14, 2023, from <https://midcdmz.nrel.gov/spa/>
- Aladin. (n.d.). *Santa Fe, NM - Climate & Monthly weather forecast*. Weather U.S. Retrieved March 14, 2023, from <https://www.weather-us.com/en/new-mexico-usa/santa-fe-climate>
- Benson, D. K., Webb, J. D., Burrows, R. W., McFadden, J. D. O., & Christensen, C. (1985). *Materials research for passive solar systems: Solid-state phase-change materials* (SERI/TR-255-1828, 5923397; p. SERI/TR-255-1828, 5923397).
<https://doi.org/10.2172/5923397>
- Bhamare, D. K., Rathod, M. K., & Banerjee, J. (2019). Passive cooling techniques for building and their applicability in different climatic zones—The state of art. *Energy and Buildings*, 198, 467–490. <https://doi.org/10.1016/j.enbuild.2019.06.023>
- Brown, A. (2023, January 9). “Green banks,” poised for billions in climate funds, draw states’ attention. The Pew Charitable Trusts.
<https://www.pewtrusts.org/en/research-and-analysis/blogs/stateline/2023/01/09/green-banks-poised-for-billions-in-climate-funds-draw-states-attention>
- Brownson, J. (n.d.). *Collector Orientation*. Solar Resource Assessment and Economics. Retrieved March 14, 2023, from <https://www.e-education.psu.edu/eme810/node/576>
- Building a Better Trombe Wall. (n.d.). *NREL Facts*.
<https://www.nrel.gov/docs/legosti/fy98/22834.pdf>
- Caridad, V., Ortiz de Zárate, J. M., Khayet, M., & Legido, J. L. (2014). Thermal conductivity and

density of clay pastes at various water contents for pelotherapy use. *Applied Clay Science*, 93–94, 23–27. <https://doi.org/10.1016/j.clay.2014.02.013>

Cellat, K., Beyhan, B., Konuklu, Y., Dündar, C., Karahan, O., Güngör, C., & Paksoy, H. (2020). 2 years of monitoring results from passive solar energy storage in test cabins with phase change materials. *Solar Energy*, 200, 29–36. <https://doi.org/10.1016/j.solener.2019.01.045>

Chavez, S. B. (n.d.). *Vision*. Mesa Del Sol. Retrieved April 25, 2023, from <https://www.mesadelsolnm.com/vision>

Climate | *Santa Fe Chamber of Commerce* | *Santa Fe, NM*. (n.d.). Santa Fe Chamber of Commerce. Retrieved March 14, 2023, from <https://www.santafechamber.com/climate.html>

Donev, J. (n.d.). *Thermal mass*. Energy Education. Retrieved March 14, 2023, from https://energyeducation.ca/encyclopedia/Thermal_mass

Energy Star. (n.d.-a). *Residential Windows, Doors and Skylights*. Energy Star. Retrieved April 25, 2023, from https://www.energystar.gov/products/res_windows_doors_skylights

Energy Star. (n.d.-b). *Super-efficient water heater*. Energy Star. Retrieved April 25, 2023, from https://www.energystar.gov/products/energy_star_home_upgrade/super_efficient_water_heater

Engineering Toolbox. (2005). *Metals, Metallic Elements and Alloys—Thermal Conductivities*. Engineering Toolbox. https://www.engineeringtoolbox.com/thermal-conductivity-metals-d_858.html

Engineering Toolbox. (2011). *Plastics—Thermal Conductivity Coefficients*. https://www.engineeringtoolbox.com/thermal-conductivity-plastics-d_1786.html

Grants.gov. (n.d.). *Grants 101*. Retrieved April 27, 2023, from <https://www.grants.gov/web/grants/learn-grants/grants-101.html>

- Harris, A. (2018, April). *Sun Intensity vs. Angle*.
<https://sciencing.com/sun-intensity-vs-angle-23529.html>
- Honsberg, C., & Bowden, S. (n.d.). *Elevation Angle*. PVEducation. Retrieved March 14, 2023,
from <https://www.pveducation.org/pvcdrom/properties-of-sunlight/elevation-angle>
- How Does a Trombe Wall Work?* | *ArchDaily*. (n.d.). Retrieved March 14, 2023, from
<https://www.archdaily.com/946732/how-does-a-trombe-wall-work>
- Hunn, B. D. (2022, March 23). Passive solar development in New Mexico. *Solar Today Magazine*.
<https://ases.org/passive-solar-development-in-new-mexico/>
- Imafidon, O. J., & Ting, D. S.-K. (2023). Retrofitting buildings with phase change materials
(PCM) – The effects of PCM location and climatic condition. *Building and Environment*,
236, 110224. <https://doi.org/10.1016/j.buildenv.2023.110224>
- Kahwaji, S., & White, M. A. (2021). Organic Phase Change Materials for Thermal Energy
Storage: Influence of Molecular Structure on Properties. *Molecules*, 26(21), Article 21.
<https://doi.org/10.3390/molecules26216635>
- Larsen, J., King, B., Kolus, H., Dasari, N., Hiltbrand, G., & Herndon, W. (2022, August 12). A
turning point for US climate progress: Assessing the climate and clean energy provisions in
the Inflation Reduction Act. *Rhodium Group*.
<https://rhg.com/research/climate-clean-energy-inflation-reduction-act/>
- Lowes. (2023, April). *8-in x 4-in Clay Red Cored Standard Brick* *Lowes.com*. Lowe's.
<https://www.lowes.com/pd/8-in-x-4-in-Clay-Red-Cored-Standard-Brick/5013595093>
- Mass Save. (n.d.-a). *About Us*. Mass Save. Retrieved April 25, 2023, from
<https://www.masssave.com/en/about-us>
- Mass Save. (n.d.-b). *Features of energy efficient homes*. Mass Save. Retrieved April 25, 2023,

from

<https://www.masssave.com/en/residential/energy-tips/features-of-energy-efficient-homes>

Mass Save. (n.d.-c). *Residential new home construction incentives*. Mass Save. Retrieved April 25, 2023, from

<https://www.masssave.com/en/residential/programs-and-services/new-construction>

McOmber, N. (2022, October 20). Inflation Reduction Act expands deductions for energy-efficient construction. *Jones & Roth CPAs & Business Advisors*.

<https://www.jrcpa.com/inflation-reduction-act-expands-deductions-for-energy-efficient-construction/>

Mhadhbi, M. (2018). *Phase Change Materials and Their Applications*.

<https://doi.org/10.5772/intechopen.71894>

Milne, R. (1921). Note on the Equation, of Time. *The Mathematical Gazette*, 10(155), 372–375.

<https://doi.org/10.1017/S0025557200232944>

Milne, R. M. (1921). Note on the Equation of Time. *The Mathematical Gazette*, 10(155), 372–375.

<https://doi.org/10.2307/3604631>

MPA. (n.d.). *Surface emissivity—Why this matters*. Retrieved April 13, 2023, from

<https://www.concretecentre.com/Performance-Sustainability/Thermal-Mass/Surface-emissivity-why-this-matters.aspx>

Nave, R. (n.d.-a). *Fresnell's Equations: Reflection and Transmission*. Retrieved March 14, 2023,

from <http://hyperphysics.phy-astr.gsu.edu/hbase/phyopt/freseq.html>

Nave, R. (n.d.-b). *Refraction of Light*. Retrieved March 14, 2023, from

<http://hyperphysics.phy-astr.gsu.edu/hbase/geoopt/refr.html#c3>

New Mexico Energy, Materials and Natural Resources Department. (n.d.-a). *ECMD Home*. New

Mexico Energy, Materials and Natural Resources Department. Retrieved April 25, 2023, from <https://www.emnrd.nm.gov/ecmd/>

New Mexico Energy, Materials and Natural Resources Department. (n.d.-b). Sustainable Building Tax Credit (SBTC). *New Mexico Energy, Materials and Natural Resources Department*. Retrieved April 25, 2023, from <https://www.emnrd.nm.gov/ecmd/tax-incentives/sustainable-building-tax-credit-sbtc/>

New Mexico Energy, Materials and Natural Resources Department. (n.d.-c). Sustainable education for advanced buildings. *New Mexico Energy, Materials and Natural Resources Department*. Retrieved April 25, 2023, from <https://www.emnrd.nm.gov/ecmd/seab/>

NREL. (n.d.). *Solar Position and Intensity*. Retrieved March 14, 2023, from <https://www.nrel.gov/grid/solar-resource/solpos.html>

NSRDB. (n.d.). Retrieved March 14, 2023, from <https://nsrdb.nrel.gov/>

Office of State and Community Energy Programs. (n.d.-a). *About the Weatherization Assistance Program*. Energy.Gov. Retrieved April 25, 2023, from <https://www.energy.gov/scep/wap/about-weatherization-assistance-program>

Office of State and Community Energy Programs. (n.d.-b). *Whole-house weatherization*. Energy.Gov. Retrieved April 25, 2023, from <https://www.energy.gov/scep/wap/whole-house-weatherization>

Passive Solar Homes. (n.d.). Energy.Gov. Retrieved March 14, 2023, from <https://www.energy.gov/energysaver/passive-solar-homes>

Pless, S., & Torcellini, P. (2004). *Trombe Walls in Low-Energy Buildings: Practical Experiences; Preprint*. <https://www.nrel.gov/docs/fy04osti/36277.pdf>

Quesada, G., Rouse, D., Dutil, Y., Badache, M., & Hallé, S. (2012). A comprehensive review of

- solar facades. Opaque solar facades. *Renewable and Sustainable Energy Reviews*, 16(5), 2820–2832. <https://doi.org/10.1016/j.rser.2012.01.078>
- Sena, S. (2021a, April 26). Solar Azimuth Angle Calculator & Solar Panels. *SolarSena*.
<https://solarsena.com/solar-azimuth-angle-calculator-solar-panels/>
- Sena, S. (2021b, April 26). Solar Hour Angle & How to Calculate it. *SolarSena*.
<https://solarsena.com/solar-hour-angle-calculator-formula/>
- Singh, S. (2020, January 12). Solar Irradiance Concepts: DNI, DHI, GHI & GTI. *Yellow Haze Solar Power*. <https://www.yellowhaze.in/solar-irradiance/>
- Solar Radiation Basics*. (n.d.). Energy.Gov. Retrieved March 14, 2023, from
<https://www.energy.gov/eere/solar/solar-radiation-basics>
- The White House. (n.d.). *Inflation Reduction Act guidebook*. The White House. Retrieved April 25, 2023, from
<https://www.whitehouse.gov/cleanenergy/inflation-reduction-act-guidebook/>
- Tycorun. (2022, May 17). *Factors Affecting Solar Radiation Energy Reaching the Earth's Surface*. Tycorun Batteries.
<https://www.tycorun.com/blogs/news/factors-affecting-solar-radiation-energy-reaching-the-earths-surface>
- Ulizio, M. (2015, August 24). *Optical Properties of Glass: How Light and Glass Interact*.
<https://www.koppglass.com/blog/optical-properties-glass-how-light-and-glass-interact>
- US Department of Energy. (n.d.). *Solar decathlon 2013*. US Department of Energy. Retrieved April 25, 2023, from https://www.solardecathlon.gov/past/2013/team_asu_unm.html
- Xin, F., & Lyu, Q. (2023). A Review on Thermal Properties of Hydrogels for Electronic Devices Applications. *Gels*, 9(1), Article 1. <https://doi.org/10.3390/gels9010007>

- Xiong, Q., Alshehri, H. M., Monfareddi, R., Tayebi, T., Majdoub, F., Hajjar, A., Delpisheh, M., & Izadi, M. (2022). Application of phase change material in improving trombe wall efficiency: An up-to-date and comprehensive overview. *Energy and Buildings*, 258, 111824. <https://doi.org/10.1016/j.enbuild.2021.111824>
- Zerubavel, E. (1982). The Standardization of Time: A Sociohistorical Perspective. *American Journal of Sociology*, 88, 1–23. <https://doi.org/10.1086/227631>

APPENDICES

Appendix A. Solar Intensity Data

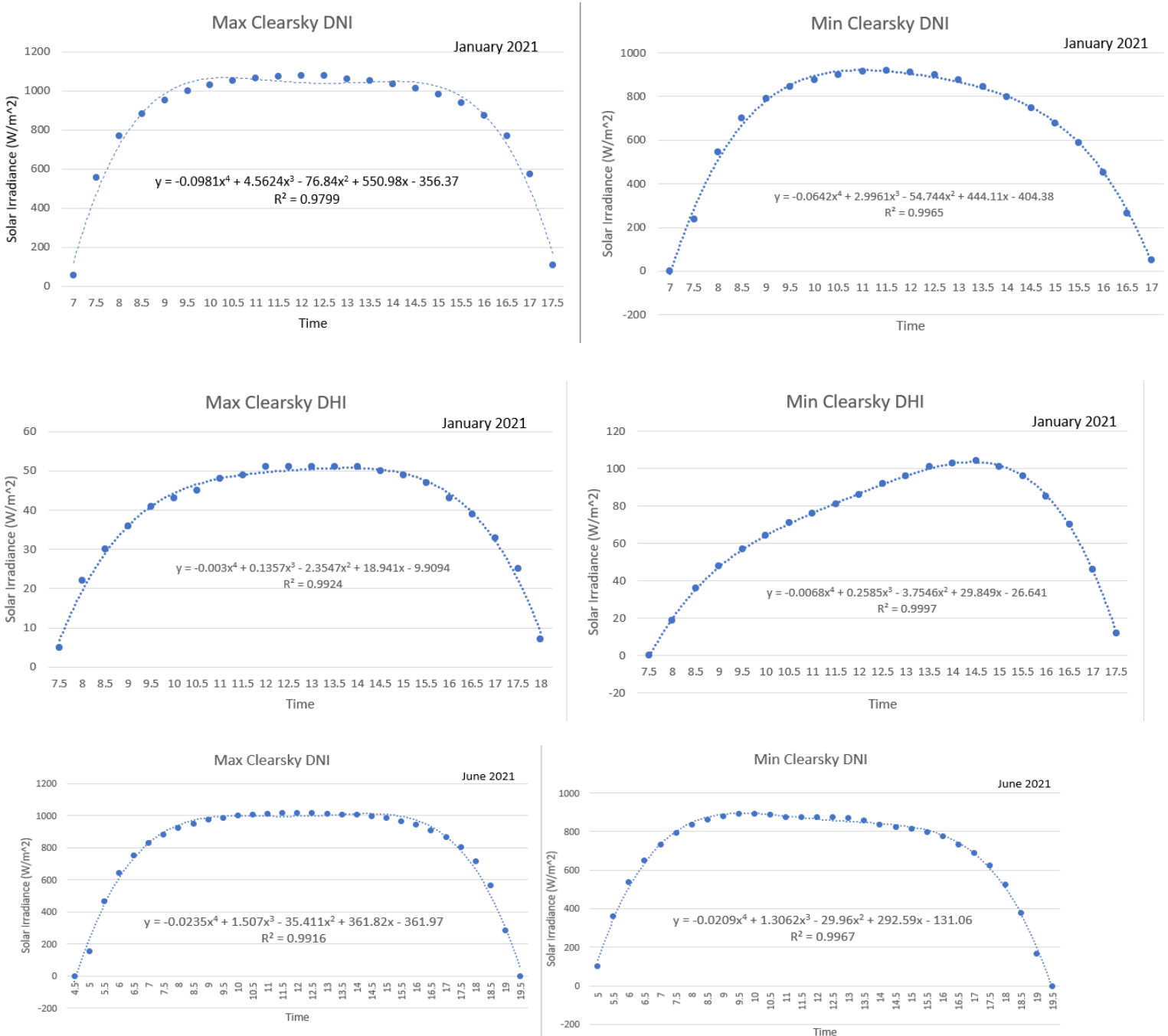
The data retrieved from NREL for the location Santa Fe, New Mexico provided us with the Clearsky DHI, Clearsky DNI and Clearsky GHI readings every 30 minutes during a 24 hour day. We manually went through each day for the entire year, highlighting the peak recording every day for each category. Shown below is an example of this process. The highlighted section on the right is the compiled data showing the peak for each day. The maximum and minimum days are then found from this information.

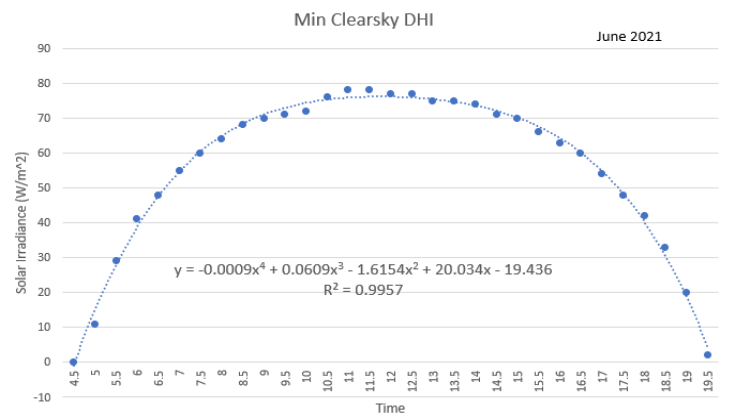
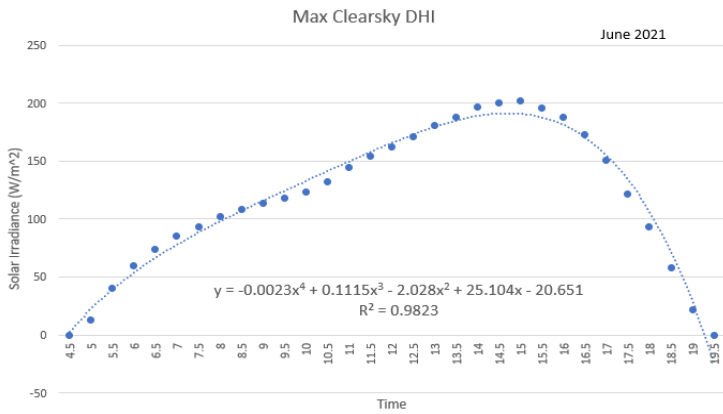
	A	B	C	D	E	F	G	H	I	J	K	L	M	N
1	Source	Location	City	State	Country	Latitude	Longitude	Time Zone	Elevation	Local Tim	Clearsky [Clearsky [Clearsky GHI Units	Dew Point Units
2	NSRDB	460709	-	-	-	35.69	-105.94	-7	2143	-7	w/m2	w/m2	w/m2	c
3	Year	Month	Day	Hour	Minute	Clearsky DHI	Clearsky DNI	Clearsky GHI	Solar Zenith Angle					
4	2021	8	1	0	0	0	0	0	126.33					
5	2021	8	1	0	30	0	0	0	126.18					
6	2021	8	1	1	0	0	0	0	125.1				Clearsky DHI	Clearsky DNI
7	2021	8	1	1	30	0	0	0	123.15			1	155	901
8	2021	8	1	2	0	0	0	0	120.41			2	164	889
9	2021	8	1	2	30	0	0	0	116.99			3	104	947
10	2021	8	1	3	0	0	0	0	113			4	128	918
11	2021	8	1	3	30	0	0	0	108.53			5	139	913
12	2021	8	1	4	0	0	0	0	103.67			6	119	933
13	2021	8	1	4	30	0	0	0	98.49			7	158	972
14	2021	8	1	5	0	0	0	0	93.07			8	234	830
15	2021	8	1	5	30	20	131	26	87.25			9	112	965
16	2021	8	1	6	0	47	354	99	81.57			10	145	884
17	2021	8	1	6	30	68	500	191	75.7			11	133	929
18	2021	8	1	7	0	85	596	292	69.72			12	112	936
19	2021	8	1	7	30	100	666	395	63.67			13	110	940
20	2021	8	1	8	0	112	716	496	57.59			14	84	984
21	2021	8	1	8	30	125	749	591	51.51			15	118	928
22	2021	8	1	9	0	139	770	679	45.48			16	142	904
23	2021	8	1	9	30	148	793	759	39.55			17	136	932
24	2021	8	1	10	0	155	809	827	33.82			18	118	931
25	2021	8	1	10	30	142	850	889	28.43			19	99	960
26	2021	8	1	11	0	120	896	941	23.65	980		20	89	990
27	2021	8	1	11	30	122	900	968	19.94	901		21	99	958
28	2021	8	1	12	0	123	901	980	18	155		22	99	984
29	2021	8	1	12	30	126	897	977	18.41			23	80	984
30	2021	8	1	13	0	126	890	957	21.03			24	78	1003
31	2021	8	1	13	30	130	874	921	25.17			25	78	1010
32	2021	8	1	14	0	135	850	870	30.19			26	91	962
33	2021	8	1	14	30	132	833	808	35.72			27	88	970
34	2021	8	1	15	0	128	811	735	41.54			28	112	950
35	2021	8	1	15	30	122	782	650	47.51			29	103	937
36	2021	8	1	16	0	116	745	558	53.57			30	97	950

Figure A1. Solar Intensity data retrieved from NREL

Appendix B. Solar Intensity Graphs and Equations

For every month of the year 2021, 4 graphs were created with the data for the max DHI, max DNI, minimum DHI and minimum DNI. In doing so, a total of 48 graphs were created. Below are the graphs for months January and February where the rest of the information for months March to December are in the tables below including the trendline equations and R² values.





DNI Max Trendline		
Month	Equation	R ² value
January	$y = -0.0981x^4 + 4.5624x^3 - 76.84x^2 + 550.98x - 356.37$	0.9799
February	$y = -0.0729x^4 + 3.6295x^3 - 65.42x^2 + 506.46x - 348.58$	0.9897
March	$y = -0.0714x^4 + 3.5817x^3 - 64.704x^2 + 496.14x - 260.09$	0.976
April	$y = -0.041x^4 + 2.3314x^3 - 48.43x^2 + 434.75x - 366.21$	0.9883
May	$y = -0.0267x^4 + 1.6191x^3 - 35.796x^2 + 339.91x - 129.6$	0.9832
June	$y = -0.0235x^4 + 1.507x^3 - 35.411x^2 + 361.82x - 361.97$	0.9916
July	$y = -0.344x^4 + 16.8x^3 - 306x^2 + 2454x - 6318$	0.987
August	$y = -0.562x^4 + 27.2x^3 - 490x^2 + 3875x - 10365$	0.986
September	$y = -0.796x^4 + 38x^3 - 676x^2 + 5296x - 14383$	0.985
October	$y = -0.988x^4 + 46.8x^3 - 827x^2 + 6464x - 17814$	0.986
November	$y = -1.48x^4 + 69.8x^3 - 1227x^2 + 9527x - 26522$	0.989
December	$y = -1.51x^4 + 72.4x^3 - 1301x^2 + 10359x - 29751$	0.991

DNI Min Trendline		
Month	Equation	R ² value
January	$y = -0.0642x^4 + 2.9961x^3 - 54.744x^2 + 444.11x - 404.38$	0.9965
February	$y = -0.0864x^4 + 3.9992x^3 - 67.364x^2 + 486.89x - 315.95$	0.9947
March	$y = -0.0407x^4 + 2.1827x^3 - 43.732x^2 + 389.51x - 354.61$	0.9952
April	$y = -0.0266x^4 + 1.6311x^3 - 37.17x^2 + 365.64x - 338.06$	0.9941
May	$y = -0.0187x^4 + 1.1069x^3 - 24.99x^2 + 258.61x - 143.1$	0.9973
June	$y = -0.0209x^4 + 1.3062x^3 - 29.96x^2 + 292.59x - 131.06$	0.9967
July	$y = 0.0275x^4 - 1.82x^3 + 26.6x^2 - 12.2x - 402$	0.995
August	$y = -0.315x^4 + 15.3x^3 - 281x^2 + 2321x - 6481$	0.995
September	$y = -0.523x^4 + 24.9x^3 - 446x^2 + 3582x - 10099$	0.998
October	$y = -0.736x^4 + 35x^3 - 625x^2 + 4950x - 13766$	0.996
November	$y = -1.37x^4 + 65.3x^3 - 1161x^2 + 9146x - 25960$	0.988
December	$y = -1.62x^4 + 77.7x^3 - 1396x^2 + 11127x - 32299$	0.994

DHI Max Trendline		
Month	Equation	R ² value
January	$y = -0.003x^4 + 0.1357x^3 - 2.3547x^2 + 18.941x - 9.9094$	0.9924
February	$y = -0.0023x^4 + 0.1021x^3 - 2.2641x^2 + 26.371x - 3.8825$	0.9954
March	$y = -0.0019x^4 + 0.1071x^3 - 2.7281x^2 + 32.562x - 22.807$	0.9952
April	$y = -0.0007x^4 + 0.0248x^3 - 0.6487x^2 + 14.534x + 9.8$	0.9967
May	$y = -0.0025x^4 + 0.1309x^3 - 2.823x^2 + 31.04x - 1.7936$	0.9983
June	$y = -0.0023x^4 + 0.1115x^3 - 2.028x^2 + 25.104x - 20.651$	0.9823
July	$y = -0.0655x^4 + 3.42x^3 - 69.3x^2 + 629x - 1828$	0.98
August	$y = 0.00163x^4 - 0.0156x^3 - 5.42x^2 + 124x - 502$	0.968
September	$y = -0.0155x^4 + 0.789x^3 - 19.6x^2 + 234x - 839$	0.997
October	$y = -0.0377x^4 + 1.83x^3 - 34.7x^2 + 301x - 889$	0.987
November	$y = -0.0504x^4 + 2.39x^3 - 43.1x^2 + 351x - 1015$	0.997
December	$y = -0.0326x^4 + 1.65x^3 - 32.5x^2 + 293x - 977$	0.982

DHI Min Trendline		
Month	Equation	R ² value
January	$y = -0.0068x^4 + 0.2585x^3 - 3.7546x^2 + 29.849x - 26.641$	0.9997
February	$y = -0.0028x^4 + 0.1205x^3 - 1.9678x^2 + 15.466x - 2.6982$	0.9936
March	$y = -0.0026x^4 + 0.1268x^3 - 2.3652x^2 + 20.208x - 7.9511$	0.9939
April	$y = -0.0014x^4 + 0.077x^3 - 1.7502x^2 + 18.675x + 6.5616$	0.991
May	$y = -0.0013x^4 + 0.0811x^3 - 2.0079x^2 + 22.454x - 21.223$	0.9937
June	$y = -0.0009x^4 + 0.0609x^3 - 1.6154x^2 + 20.034x - 19.436$	0.9957
July	$y = -0.9273x^4 + 1.33x^3 - 24.6x^2 + 204x - 551$	0.994
August	$y = -0.0274x^4 + 1.29x^3 - 23.2x^2 + 189x - 519$	0.996
September	$y = -0.0355x^4 + 1.66x^3 - 29.5x^2 + 237x - 659$	0.996
October	$y = -0.0317x^4 + 1.49x^3 - 26.6x^2 + 216x - 617$	0.995
November	$y = -0.0338x^4 + 1.62x^3 - 29.7x^2 + 245x - 723$	0.994
December	$y = -0.0346x^4 + 1.62x^3 - 29.1x^2 + 236x - 689$	0.998

Appendix C. Composite Mold Details

The following figure and table detail the design and dimensions of our composite brick mold, made with wood and screws.

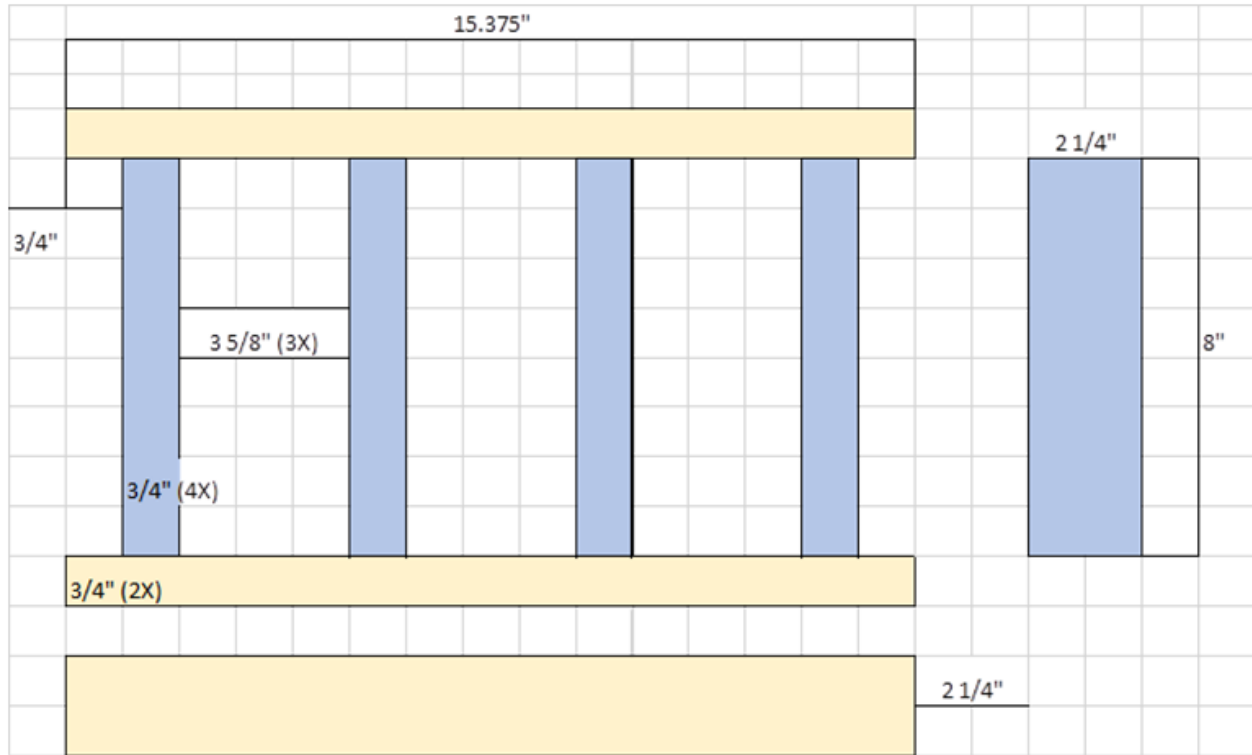


Figure C1. Design of Brick Mold with Dimensions

Table C1. Material List for Wood used for Brick Mold

Description	Length	Width	Thickness	Quantity
Board 1, blue	8"	2.25"	0.75"	4
Board 2, yellow	15.375"	2.25"	0.75"	2

Appendix D. Testing Apparatus Details

D1. Arduino Code for Testing Apparatus

```
#include <Wire.h>
// by John Sullivan and Ahmet Can Sabuncu, ME3902 Summer 2021
//
#include <Adafruit_ADS1X15.h> // same library for both the ads1015 and ads1115
Adafruit_ADS1115 ads1115_1; // Declare an instance of the ADS1115 at address slot 0x48
Adafruit_ADS1115 ads1115_2; // Declare an instance of the ADS1115 at address slot 0x4A
Adafruit_ADS1115 ads1115_3; // Declare an instance of the ADS1115 at address slot 0x4B

int16_t rawADCvalue; // The is where we store the value we receive from the ADS1115
int16_t rawADCvalue2; //Second thermocouple
int16_t rawADCvalue3; //Third thermocouple
int16_t rawADCvalue4; //Fourth thermocouple
int16_t rawADCvalue5; //Fifth thermocouple
    // int16_t is a 16 bit signed integer range = -32768 to +32767
    // scalefactor = max Voltage / ( 2^15)-1 = max Voltage/(32767) for 16 bit with most
    // significant bit reserved for sign (+ or -)

float volts = 0.0; // The result of applying the scale factor to the raw value
float volts2 = 0.0; //Second thermocouple in A2 and A3 pins
float volts3 = 0.0; //Third thermocouple in A0 and A1 pins
float volts4 = 0.0; //Fourth thermocouple in A2 and A3 pins
float volts5 = 0.0; //Fifth thermocouple in A0 and A1 pins
float bit_res = 0.0078125; // This is the bit resolution in [mV] will change with the gain, please refer
to the table below

float uV = 0.0; // This is just volts times a million [uV]
float uV2 = 0.0; // Second thermocouple
float uV3 = 0.0; // Third thermocouple
float uV4 = 0.0; // Fourth thermocouple
float uV5 = 0.0; // Fifth thermocouple

float a0 = 0, a1 = 1.978425e-2, a2 = -2.001204e-7, a3 = 1.036969e-11; // These are the NIST coefficients
for converting voltage readings to temperature, link below
float a4 = -2.549687e-16, a5 = 3.585153e-21, a6 = -5.344285e-26;
//https://srdata.nist.gov/its90/type_t/tcoefficients_inverse.html

float TempDegC=0;
float TempDegC2=0; // Reading off of second thermocouple
float TempDegC3=0; // Reading off of third thermocouple
float TempDegC4=0; // Reading off of fourth thermocouple
float TempDegC5=0; // Reading off of fifth thermocouple

unsigned long StartTime = 0;
// // Gain Max Volt ads1015 ads1115
// ads1115.setGain(GAIN_TWOTHIRDS); // 2/3x gain +/- 6.144V 1 bit = 3mV (default) 1 bit = 187.5
micro-V
// ads1015.setGain(GAIN_ONE); // 1x gain +/- 4.096V 1 bit = 2mV 1 bit = 125. micro-V
```

```

// ads1015.setGain(GAIN_TWO); // 2x gain +/- 2.048V 1 bit = 1mV 1 bit = 62.5 micro-V
// ads1015.setGain(GAIN_FOUR); // 4x gain +/- 1.024V 1 bit = 0.5mV 1 bit = 31.25 micro-V
// ads1015.setGain(GAIN_EIGHT); // 8x gain +/- 0.512V 1 bit = 0.25mV 1 bit = 15.625 micro-V
// ads1015.setGain(GAIN_SIXTEEN); // 16x gain +/- 0.256V 1 bit = 0.125mV 1 bit = 7.8125 micro-V
//
void setup(void)
{
  Serial.begin(9600);
  ads1115_1.setGain(GAIN_SIXTEEN); // Set gain to 16x
  ads1115_2.setGain(GAIN_SIXTEEN); // Set gain to 16x
  ads1115_3.setGain(GAIN_SIXTEEN); // Set gain to 16x

  ads1115_1.begin(0x48); //address to 1st ADC chip where ADDR = GND
  ads1115_2.begin(0x4A); //address to 2nd ADC chip where ADDR = SDA
  ads1115_3.begin(0x4B); //address to 3rd ADC chip where ADDR = SCL
  // start a timer
  StartTime = millis();
}

void loop(void)
{
  rawADCvalue = ads1115_1.readADC_Differential_0_1(); // Differential voltage measurement between A0
and A1 on the FIRST ADC chip
  rawADCvalue2 = ads1115_1.readADC_Differential_2_3(); //Differential voltage measurement between
A2 and A3 on the FIRST ADC chip
  rawADCvalue3 = ads1115_2.readADC_Differential_0_1(); // Differential voltage measurement between
A0 and A1 on the SECOND ADC chip
  rawADCvalue4 = ads1115_2.readADC_Differential_2_3(); //Differential voltage measurement between
A2 and A3 on the SECOND ADC chip
  rawADCvalue5 = ads1115_3.readADC_Differential_0_1(); // Differential voltage measurement between
A0 and A1 on the THIRD ADC chip

  volts = rawADCvalue * bit_res; // Convert rawADC number to voltage in [mV] on thermocouples 1 - 5
  volts2 = rawADCvalue2 * bit_res;
  volts3 = rawADCvalue3 * bit_res;
  volts4 = rawADCvalue4 * bit_res;
  volts5 = rawADCvalue5 * bit_res;

  uV = volts*1e3; // Express the voltage in microVolts
  uV2 = volts2*1e3;
  uV3 = volts3*1e3;
  uV4 = volts4*1e3;
  uV5 = volts5*1e3;

  TempDegC = a0 + a1*uV + a2*pow(uV,2) + a3*pow(uV,3) + a4*pow(uV,4) + a5*pow(uV,5) +
a6*pow(uV,6);
  TempDegC2 = a0 + a1*uV2 + a2*pow(uV2,2) + a3*pow(uV2,3) + a4*pow(uV2,4) + a5*pow(uV2,5) +
a6*pow(uV2,6);
  TempDegC3 = a0 + a1*uV3 + a2*pow(uV3,2) + a3*pow(uV3,3) + a4*pow(uV3,4) + a5*pow(uV3,5) +
a6*pow(uV3,6);

```

```

TempDegC4 = a0 + a1*uV4 + a2*pow(uV4,2) + a3*pow(uV4,3) + a4*pow(uV4,4) + a5*pow(uV4,5) +
a6*pow(uV4,6);
TempDegC5 = a0 + a1*uV5 + a2*pow(uV5,2) + a3*pow(uV5,3) + a4*pow(uV5,4) + a5*pow(uV5,5) +
a6*pow(uV5,6);

```

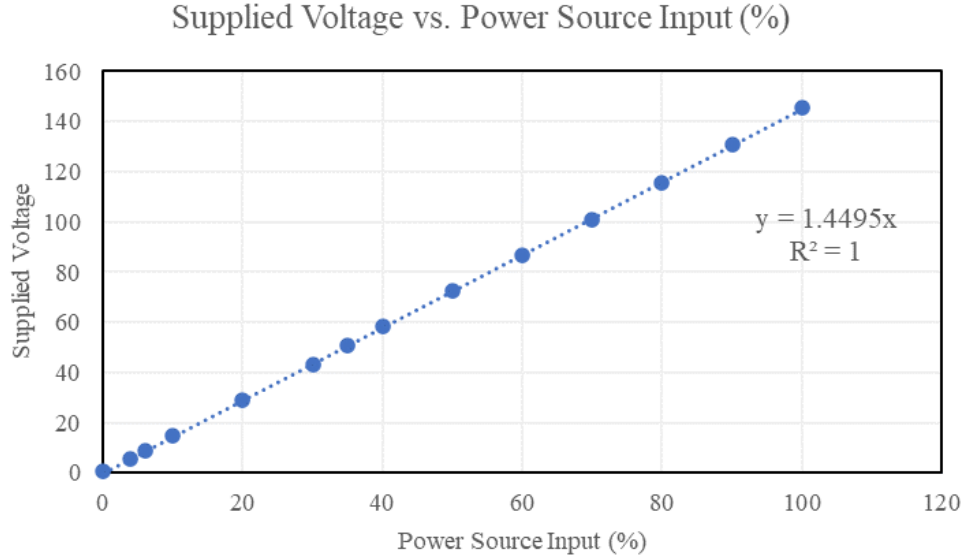
```

unsigned long CurrentTime = millis();
float ElapsedTime = (CurrentTime-StartTime)/1000.0;
// Serial.print(++rowNumber);
// Serial.print("Time (sec) ");
Serial.print(ElapsedTime,3);
Serial.print(",");
// Serial.print("microVolts Measured\tTemperature (deg C): ");
//Serial.print("\n");
Serial.print(uV,2);
Serial.print(",");
Serial.print(TempDegC,2);
Serial.print(",");
Serial.print(uV2,2);
Serial.print(",");
Serial.print(TempDegC2,2);
Serial.print(",");
Serial.print(uV3,2);
Serial.print(",");
Serial.print(TempDegC3,2);
Serial.print(",");
Serial.print(uV4,2);
Serial.print(",");
Serial.print(TempDegC4,2);
Serial.print(",");
Serial.print(uV5,2);
Serial.print(",");
Serial.println(TempDegC5,2);
//Serial.println(",");
delay(500);
}

```

//3-20 Working with ArduSpreadsheet : <https://circuitjournal.com/arduino-serial-to-spreadsheet>
//Install Adafruit_ADS1X15.h in Tools/Manage Libraries
//Make sure to have reference ends in ice slurry at 0deg C - keep at 0 using thermometer
//check for vampire connections - if any of the temperatures are negative, just switch the A pins
//label thermocouples

D2. Calibration Curve for Heating Pad



D3. Testing Setup and Procedure

1. Set up apparatus (insulation chamber with stand, thermocouples are in an ice bath and attached to Arduino, voltage source connected to heating pad)
 - a. Test the voltage source to ensure it supplies 0.25 A to the heating pad, corresponding to 28 V (power source setting of 20%)
 - b. Confirm each thermocouple is calibrated and provides a reading
 - c. The heating pad is sufficiently heated prior to testing to the settings mentioned above
2. Place the heating pad onto the metal stand and close chamber. Turn on the power source to 20% and allow the metal stand to come to temperature equilibrium with the heating pad. This corresponded to about 7 minutes of the heating pad running with no brick in the chamber.
3. Place a brick on the stand, contacting the heating pad on its 2-1/4" high and 7-5/8" long side
4. Insert labeled thermocouples into holes within the brick, between the heating pad and brick, and inside the insulated chamber.
5. Close the insulation chamber and run the Arduino code that logs time and temperature data.
6. Stop collecting data when the outermost thermocouple in the brick reaches a stable 25°C.
7. Export temperature versus time data from Arduino into Excel and save.

Appendix E. Sample Calculations for Heat Capacity

E1. Volume Percentage of Material in Bricks

Modular Brick Volume

The typical modular brick has three holes. Our team could not find a universal diameter for these holes, but estimated them to be 1 in. The dimensions for a modular brick are 8" by 5³/₈" by 2¹/₄".

$$\text{Total Brick Volume: } V = l * w * h = 101.25 \text{ in}^3 = 1660 \text{ cm}^3$$

$$\text{Volume of Holes: } V = 3\text{holes} * \pi r^2 h = 13.3 \text{ in}^3 = 0.15 \text{ cm}^3$$

$$\text{Hole Volume Percentage} = 15\%$$

Volume Percentage of Material in Brick

To calculate the volume percentage of the material in the brick, the following process was followed. These sample calculations are for the brick with 1.0 cm tubing and gel material.

Tubing ID (cm)	0.9
Inner Radius (cm)	0.45
Tubing OD (cm)	1
Outer Radius	0.5
Tubing Height (cm)	5.08
Number of Tubes	26

$$\text{Volume of Material: } V_m = (\# \text{ tubes})\pi r^2 h = 84.03 \text{ cm}^3$$

$$\text{Volume of Tubing \& Material: } V_{t,m} = (\# \text{ tubes})\pi r^2 h = 103.7 \text{ cm}^3$$

$$\text{Volume of Cement: } V_c = V_{brick} - V_{t,m} = 1555 \text{ cm}^3$$

$$\text{Material Volume Percentage} = 6.7\%$$

E2. Heat Capacity of Composite Brick

The heat capacity of the composite brick was determined using an overall energy balance for the system. These sample calculations are representative of the brick 1.0 cm tubing and gel material.

$$\text{Energy Balance: } Q_H = Q_{air} + Q_{brick} + Q_i$$

$$Q_H = m_{air} c_{p,air} \Delta T + m_{brick} c_{p,brick} \Delta T + U_i A \Delta T_{LM} t$$

Energy Supplied by Heating Pad

$$Q_H = \text{Voltage} * \text{Current} * \text{Total Time} = (120V) * (0.25A) * (2878.016s)$$

$$Q_H = 86,340 J = 86.340 kJ$$

Note: Here voltage is the voltage capacity of the heating pad from the manufacturer, corresponding to a power source input of 100%, which is 120V. Current was measured using an ammeter. Total time is the total run time of the trial.

Heat Absorbed by Air in Chamber

$$Q_{air} = m_{air} c_{p,air} \Delta T = (0.0118 kg) * (1.006 \frac{kJ}{kg C}) * (28.66 - 23.38C)$$

$$Q_{air} = 62.927 J = 0.063 kJ$$

Note: Mass of air was determined by multiplying the inner volume of the chamber, 0.009m³, by the density of air, 1.293 kg/m³.

Heat Absorbed by Insulation

$$Q_i = UA\Delta T_{LM} t = (0.057 \frac{W}{m^2 K}) * (0.309m^2) * (0.001K) * (2878.016s)$$

$$Q_i = 5.076 J = 0.005 kJ$$

Heat Absorbed by Brick and Heat Capacity

$$Q_{brick} = m_{brick} c_{p,brick} \Delta T \rightarrow c_{p,brick} = \frac{(Q_H - Q_{air} - Q_i)}{m_{brick} \Delta T} = \frac{86.27 kJ}{(2.47kg)*(28.26K)}$$

$$c_{p,brick} = 1.236 \frac{kJ}{kg K}$$

% Increase of Heat Capacity

To further understand the increase in heat capacity depending on material or tubing size, we calculated the percent increase of each trial compared to the control brick.

$$c_{p,control} = 1.190 \frac{kJ}{kg K}$$

$$c_{p,brick} = 1.236 \frac{kJ}{kg K}$$

$$\% Inc. = \frac{c_{p,brick} - c_{p,control}}{c_{p,control}} * 100 = 3.84\%$$

Appendix F. MATLAB Flux Time Curve Generation Code

```
%% Control Section
%-----
%this is the code block to run it
clc
clear all;
    %time and data range
    startdate = "12/01/2023"; %mm/dd/yyyy
    starttime = "03:00"; %'hh:mm' from 00:00-24:00
    enddate = "12/02/2023"; %mm/dd/yyyy
    endtime = "03:00"; %'hh:mm' from 00:00-24:00
    numpoints = 201;
    %location inputs
    timezonedif = "-07:00"; %"+-00:00 from UTC"
    long = -105.944183;%degrees East or - degrees West
    lat = 35.691544;%degrees North or - degrees south
    %wall orientation
    tilt = 90; %angle between horizontal and wall, 90 for vertical
    colaz = 0; %collector azimuth angle, measured from S, W is positive
        %such that South =0, West=90

    %refractive indexes
    nair = 1.0003;
    nglass = 1.52;

%finding hemispherical transmissivity
summing = 0;
num = 0;
for i=0:1:90
    trans_temp = find_transmit_by_angle(nair, nglass, i);
    summing = summing + trans_temp;
    num = num + 1;
end
%averaging the sum of the step integral to find the hemispherical
%transmissivity
trans_hemi = summing/num;

[azimuths, zeniths, angleincs, directavgs, diffuseavgs, timesecs] = generatetarttoend(startdate, starttime,
enddate, endtime, numpoints, timezonedif, long, lat, tilt, colaz);
%-----
%finding transmissivity for each angle of incidence
trans_directs = zeros(length(angleincs), 1);
%will default to NaN answers if numpoints is 1
for i=1:length(trans_directs)
```

```

    trans_directs(i) = find_transmit_by_angle(nair, nglass, angleincs(i));
end

%applying transmissivities and summing to find total transmitted intensity
%for each time
transintens = zeros(length(directavgs), 1);
for i=1:length(directavgs)
    thrudirect = trans_directs(i)*directavgs(i);
    thrudiffuse = trans_hemi*diffuseavgs(i);
    transintens(i) = thrudirect + thrudiffuse;
end

generatetxtfile(timesecs, transintens, startdate, starttime, endtime, long, lat);
%%
%Plotting the Rays

% %plotting a ray from zenith and azimuth angle- 3d
% point = [sind(azimuth), cosd(azimuth), cosd(zenith)];
% origin = [0,0,0];
% figure;hold on;
% plot3([origin(1) point(1)], [origin(2) point(2)], [origin(3) point(3)], '--','LineWidth', 3);
% plot3([origin(1)], [origin(2)], [origin(3)], '>', 'LineWidth', 3);
% grid on;
% xlabel('East'), ylabel('North'), zlabel('Sky')
% set(gca, 'CameraPosition', [5, -20, 10]);

%plotting a 3d surface over a range of stuff
clf
figure(1); hold on;
x = sind(azimuths);
y = cosd(azimuths);
z = cosd(zeniths);
xv = linspace(min(x), max(x), 20);
yv = linspace(min(y), max(y), 20);
[X,Y] = meshgrid(xv, yv);
Z = griddata(x,y,z,X,Y);

stem3(x,y,z, 'filled', '-or', 'LineWidth', 2)
grid on;

xlim([-1 1])
ylim([-1 1])
zlim([-1 1])

```

```

[xs ys] = meshgrid(-1:0.1:1);
zs = zeros(size(xs,1));
%% xs = linspace(-1, 1, 2);
%% ys = linspace(-1, 1, 2);
% [xs, ys] = meshgrid(xv, xv);
% zs = zeros(length(ys), length(xs));
% surf(xs,ys,zs, 'FaceAlpha', 0.3);
surf(xs, ys, zs, 'FaceAlpha', 0.2);
set(gca, 'CameraPosition', [1, -1, 1]);
hXL=xlabel('East');
hXL.Position=hXL.Position+[1 1.5 0];
hYL=ylabel('North');
hYL.Position=hYL.Position+[-2 3 0];
% for i=1:36
%   camorbit(10,0)
%   drawnow
%   pause(0.5);
% end

```

%% Functions

```

function generatetxtfile (timesecs, transintens, date, starttime, endtime, long, lat)
%find the month name as a string
themoth = datetime(date, "Format", "MM/dd/uuu");
themoth = month(themoth, "shortname");
themoth = string(themoth);
%convert colons in times to '.' as filenames cant contain colons
starttime = strrep(starttime, ':', '.');
endtime = strrep(endtime, ':', '.');
%long lat string
long = string(long);
lat = string(lat);
longlat = append("long=", long, " lat=", lat);
%find step size
stepsz = timesecs(2) - timesecs(1);
stepsz = string(stepsz);
stepstr = append("step=", stepsz, "sec");
%create name string
name = append(themoth, ", ", starttime, " to ", endtime, " at ", longlat, ", ", stepstr, ".dat");
%create and print the outputs
timesecs = transpose(timesecs);
transintens = transpose(transintens);

```

```

A = [timesecs; transintens];
fileID = fopen(name, 'w+');
fprintf(fileID, '%12.2f %12.8f\n', A);
fclose(fileID);
end

```

```

function [azimuths, zeniths, angleincs, directavgs, diffuseavgs, timesecs] = generatetarttoend(startdate,
starttime, enddate, endtime, numpoints, timezonedif, long, lat, tilt, colaz)

```

```

start = datetime(startdate, "InputFormat", "MM/dd/yyyy") + duration(starttime, 'InputFormat', 'hh:mm',
'Format', 'h');
theend = datetime(enddate, "InputFormat", "MM/dd/yyyy") + duration(endtime, 'InputFormat', 'hh:mm',
'Format', 'h');
thelength = theend - start;
step = thelength/(numpoints - 1);

```

```

timesecs = maketimearr(start, theend, numpoints);

```

```

% duration("14:20", 'InputFormat','hh:mm', "Format", 'h')
azimuths = zeros(numpoints, 1);
zeniths = zeros(numpoints, 1);
angleincs = zeros(numpoints, 1);
directavgs = zeros(numpoints, 1);
diffuseavgs = zeros(numpoints, 1);
timesecs = zeros(numpoints, 1);
for i = 1:numpoints
    dateandtime = start + (i - 1)*step;
    datepres = datetime(dateandtime, 'InputFormat',"MM/dd/yyyy hh:mm", "Format", 'MM/dd/yyyy');
    timepres = datetime(dateandtime, 'InputFormat',"MM/dd/yyyy hh:mm", "Format", 'HH:mm');
    timepres = string(timepres, 'HH:mm');
    [azimuths(i), zeniths(i), angleincs(i)] = azimuthzenith(datepres, timepres, timezonedif, long, lat, tilt,
colaz);
    [directavgs(i), diffuseavgs(i)] = findintens(datepres, timepres);
end
end

```

```

function trans_frac = find_transmit_by_angle(n1, n2, theta1)
    %theta1 is the angle of incidence, n1 is the index of refraction of
    %incident medium, n2 is index of refraction of transmitting medium

    %slightly adjust theta1 if its 0 or 90 degrees as if it is

```

```

if theta1 == 0
    theta1 = theta1 + 0.0001;
end
if theta1 == 90
    theta1 = theta1 + 0.0001;
end

%find the transmitted angle
theta2 = asind(n1/n2*sind(theta1));
%find parallel and perpendicular fractional transmissivity amplitudes
tpar = (2*sind(theta2)*cosd(theta1))/(sind(theta1+theta2)*cosd(theta1-theta2));
tperp = (2*sind(theta2)*cosd(theta1))/sind(theta1+theta2);
%find the parallel and perpendicular transmitted energy fraction
tau_par = tpar^2*(n2*cosd(theta2))/(n1*cosd(theta1));
tau_perp = tperp^2*(n2*cosd(theta2))/(n1*cosd(theta1));
%find the net transmitted energy fraction
tau_net = (tau_par+tau_perp)/2;
trans_frac = tau_net;

%if the angle of incidence is greater than 90 degrees there is no
%transmission
if abs(theta1) > 90
    trans_frac = 0;
end
end

function [azimuth, zenith, angleinc] = azimuthzenith(date, time, timezonedif, long, lat, tilt, colaz)

%%converting inputs
date = datetime(date, "InputFormat", "MM/dd/yyyy");

time = duration(time, 'InputFormat', 'hh:mm', 'Format', 'h');

timezonedif = duration(timezonedif, 'InputFormat', 'hh:mm');
UTctime = time + timezonedif;
UTctimedayfrac = duration(UTctime, 'Format', 'd');
%%finding day
d = day(date, "dayofyear") - 1 + (UTctimedayfrac);
d = days(d);
%%finding hour angle
%local standard time meridian
LSTM = 15 * hours(timezonedif); %degrees

```

```

%equation of time
B = 360/365*(d - 81);%degrees
EoT = 9.87*sind(2*B) - 7.53*cosd(B) - 1.5*sind(B); %minutes
%time correction factor
TC = 4*(long - LSTM) + EoT; %minutes
%local solar time
LST = hours(time) + TC/60; %hours decimal format
%hour angle
h = 15*(LST - 12); %degrees
%%finding angle
%declination angle
delta = -23.44*cosd((360/365)*(d + 10)); %degrees
%solar zenith angle
zenith = acosd(sind(lat)*sind(delta) + cosd(lat)*cosd(delta)*cosd(h)); %degrees
%solar azimuth angle
azimuth = acosd((sind(delta)*cosd(lat) - cosd(h)*cosd(delta)*sind(lat))/(sind(zenith))); %degrees

if LST > 12
    %once past solar noon the azimuth angle fomrulas output westward from
    %N, so adjust to be eastward from N (validated against NREL data)
    azimuth = 360 - azimuth;
end

%finding angle of incidence
angleinc =
acosd((sind(lat)*sind(delta)*cosd(tilt))-cosd(lat)*sind(delta)*sind(tilt)*cosd(colaz)+cosd(lat)*cosd(delta)*c
osd(tilt)*cosd(h)+sind(lat)*cosd(delta)*sind(tilt)*cosd(colaz)*cosd(h)+cosd(delta)*sind(tilt)*sind(colaz)*si
nd(h));
end

function timesecs2 = maketimearr(start, theend, numpoints)
    difference = theend - start;
    difinsecs = seconds(difference);
    secstep = difinsecs / (numpoints - 1);

    timesecs = zeros(numpoints, 1);

%   timesecs(1) = 0;
    for i = 1:numpoints
        timesecs(i) = 0 + secstep*(i-1);
    end

    timesecs2 = timesecs;
end

```

```

function [directavg, diffuseavg] = findintens(datepres, timepres)
    %convert the timepres to hours
    timehrs = duration(timepres, 'InputFormat', 'hh:mm', 'Format', 'h');
    timehrs = hours(timehrs);
    %if the time is longer than 24 (overrun the day) set it back
    %to being relative to the start of a day
    if timehrs > 24
        timehrs = timehrs - 24;
    end

    month = datetime(datepres, 'InputFormat', 'MM/dd/yyyy', 'Format', 'MM');
    month = string(month);
    t = timehrs; %for ease of use
    if month == "01"
        %january
        directmin = -0.0642*t^4+2.9961*t^3-54.744*t^2+444.11*t-404.38;
        directmax = -0.0981*t^4+4.5624*t^3-76.84*t^2+550.98*t-356.37;
        diffusemin = -0.0068*t^4+0.2585*t^3-3.7546*t^2+29.849*t-26.641;
        diffusemax = -0.003*t^4+0.1357*t^3-2.3547*t^2+18.941*t-9.9094;
    elseif month == "02"
        %february
        directmin = -0.0864*t^4+3.9992*t^3-67.364*t^2+486.89*t-315.95;
        directmax = -0.0729*t^4+3.6295*t^3-65.42*t^2+506.46*t-348.58;
        diffusemin = -0.0028*t^4+0.1205*t^3-1.9678*t^2+15.466*t-2.6982;
        diffusemax = -0.0023*t^4+0.1021*t^3-2.2641*t^2+26.371*t-3.8825;

    elseif month == "03"
        %march
        directmin = -0.0407*t^4+2.1827*t^3-43.732*t^2+389.51*t-354.61;
        directmax = -0.0714*t^4+3.5817*t^3-64.704*t^2+496.14*t-260.009;
        diffusemin = -0.0026*t^4+0.1268*t^3-2.3652*t^2+20.208*t-7.9511;
        diffusemax = -0.0019*t^4+0.1071*t^3-2.7281*t^2+32.562*t-22.807;

    elseif month == "04"
        %april
        directmin = -0.0266*t^4+1.6311*t^3-37.17*t^2+365.64*t-338.06;
        directmax = -0.041*t^4+2.3314*t^3-48.43*t^2+434.75*t-366.21;
        diffusemin = -0.0014*t^4+0.077*t^3-1.7502*t^2+18.675*t+6.5616;
        diffusemax = -0.0007*t^4+0.0248*t^3-0.6487*t^2+14.534*t+9.8;

    elseif month == "05"
        %may
        directmin = -0.0187*t^4+1.1069*t^3-24.99*t^2+258.61*t-143.1;

```

```

directmax = -0.0267*t^4+1.691*t^3-35.796*t^2+339.91*t-129.6;
diffusemin = 0.0013*t^4+0.0811*t^3-2.0079*t^2+22.454*t-21.223;
diffusemax = -0.0025*t^4+0.1309*t^3-2.823*t^2+31.04*t-1.7936;

elseif month == "06"
    %june
    directmin = -0.0209*t^4+1.3062*t^3-29.96*t^2+292.59*t-131.06;
    directmax = -0.0235*t^4+1.507*t^3-35.411*t^2+361.82*t-361.97;
    diffusemin = -0.0009*t^4+0.0609*t^3-1.6154*t^2+20.034*t-19.436;
    diffusemax = -0.0023*t^4+0.1115*t^3-2.028*t^2+25.104*t-20.651;

elseif month == "07"
    %july
    directmin = -402-12.2*t+26.6*t^2-1.82*t^3+0.0275*t^4;
    directmax = -6318+2454*t-306*t^2+16.8*t^3-0.344*t^4;
    diffusemin = -551+204*t-24.6*t^2+1.33*t^3-0.0273*t^4;
    diffusemax = -1828+629*t-69.3*t^2+3.42*t^3-0.0655*t^4;

elseif month == "08"
    %august
    directmin = -6481+2321*t-281*t^2+15.3*t^3-0.315*t^4;
    directmax = -10365+3875*t-490*t^2+27.2*t^3-0.562*t^4;
    diffusemin = -519+189*t-23.2*t^2+1.29*t^3-0.0274*t^4;
    diffusemax = -502+124*t-5.42*t^2-0.0156*t^3+0.00163*t^4;

elseif month == "09"
    %september
    directmin = -10099+3582*t-446*t^2+24.9*t^3-0.523*t^4;
    directmax = -14383+5296*t-676*t^2+38*t^3-0.796*t^4;
    diffusemin = -659+237*t-29.5*t^2+1.66*t^3-0.0355*t^4;
    diffusemax = -839+234*t-19.6*t^2+0.789*t^3-0.0155*t^4;

elseif month == "10"
    %october
    directmin = -13766+4950*t-625*t^2+35*t^3-0.736*t^4;
    directmax = -17814+6464*t-827*t^2+46.8*t^3-0.988*t^4;
    diffusemin = -617+216*t-26.6*t^2+1.49*t^3-0.0317*t^4;
    diffusemax = -889+301*t-34.7*t^2+1.83*t^3-0.0377*t^4;

elseif month == "11"
    %november
    directmin = -25960+9146*t-1161*t^2+65.3*t^3-1.37*t^4;
    directmax = -26522+9527*t-1227*t^2+69.8*t^3-1.48*t^4;
    diffusemin = -723+245*t-29.7*t^2+1.62*t^3-0.0338*t^4;

```

```

diffusemax = -1015+351*t-43.1*t^2+2.39*t^3-0.0504*t^4;

elseif month == "12"
    %december
    directmin = -32299+11127*t-1396*t^2+77.7*t^3-1.62*t^4;
    directmax = -29751+10359*t-1301*t^2+72.4*t^3-1.51*t^4;
    diffusemin = -689+236*t-29.1*t^2+1.62*t^3-0.0346*t^4;
    diffusemax = -937+293*t-32.5*t^2+1.65*t^3-0.0326*t^4;

end

directavg = (directmin + directmax) /2;
diffuseavg = (diffusemin + diffusemax) /2;
%since the equations are parabolas generated from the data for which
%the intensities are not zero they may generate negative numbers for
%other times (around when the sun is below the horizon), if they do, set them to 0
if directavg < 0
    directavg = 0;
end
if diffuseavg < 0
    diffuseavg = 0;
end
end
end

```

Appendix G. Simulation Results Data

	Energy out of the brick between "sunset" and 3AM [J]			
Month	Basic Bricks	Small Tube PCM Bricks	Medium Tube PCMBricks	Large Tube PCM Bricks
Jan	38,703	40,847	40,548	43,019
Feb	45,932	48,380	48,039	50,850
Mar	54,071	56,729	56,359	59,405
Apr	54,660	57,225	56,868	59,802
May	51,164	52,724	52,495	54,562
Jun	39,811	41,441	41,215	43,056
Jul	44,009	45,772	45,528	47,523
Aug	44,064	46,072	45,793	48,079
Sep	48,191	50,580	50,248	52,981
Oct	43,614	46,028	45,691	48,467
Nov	52,766	55,516	55,133	58,286
Dec	49,088	51,560	51,216	54,046

Table F1. Raw data for energy released from the different bricks between a time of lowered solar intensity and 3AM for each month.

	Percent Increase of Energy Leaving the Brick Between "sunset" and 3AM Compared to Basic Bricks		
Month	Small Tube PCM Bricks	Medium Tube PCM Bricks	Large Tube PCM Bricks
Jan	5.54%	4.77%	11.15%
Feb	5.33%	4.59%	10.71%
Mar	4.92%	4.23%	9.86%
Apr	4.69%	4.04%	9.41%
May	3.05%	2.60%	6.64%
Jun	4.09%	3.53%	8.15%
Jul	4.01%	3.45%	7.98%
Aug	4.56%	3.92%	9.11%
Sep	4.96%	4.27%	9.94%
Oct	5.53%	4.76%	11.13%
Nov	5.21%	4.49%	10.46%
Dec	5.04%	4.34%	10.10%
Average:	4.74%	4.08%	9.55%

Table F2. Percent increases of energy released from the PCM bricks between a time of lowered solar intensity and 3AM relative to a standard Trombe wall brick for each month.